Extreme erosion on high-energy embayed beaches: influence of megarips and storm grouping

Carlos Loureiro [a*]

Óscar Ferreira [a]

Andrew Cooper [b]

[a] CIMA, Centre for Marine and Environmental Research, Universidade do Algarve, Campus de Gambelas, Faro 8005-139, Portugal

[b] Centre for Coastal and Marine Research, School of Environmental Sciences, University of Ulster, Cromore Road, Coleraine BT52 1SA, Northern Ireland, UK

* Corresponding author

Email:carlos.loureiro@stir.ac.uk, oferreir@ualg.pt , jag.cooper@ulster.ac.uk

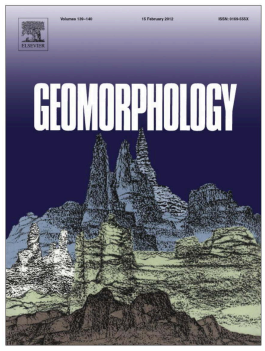

Published in:

Geomorphology

Volume 139-140, February 2012, Pages 155-171

DOI: 10.1016/j.geomorph.2011.10.013

URL: https://www.sciencedirect.com/science/article/pii/S0169555X11005290

Geomorphology 139-140 (2012) 155–171

Contents lists available at SciVerse ScienceDirect

Geomorphology

journal homepage: www.elsevier.com/locate/geomorph

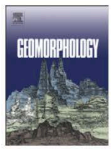

Extreme erosion on high-energy embayed beaches: Influence of megarips and storm grouping

Carlos Loureiro [a,*], Óscar Ferreira [a], J. Andrew G. Cooper [b]

[a] CIMA, Centre for Marine and Environmental Research, Universidade do Algarve, Campus de Gambelas, Edifício 7, 8005-139 Faro, Portugal

[b] Centre for Coastal and Marine Research, School of Environmental Sciences, University of Ulster, Cromore Road, Coleraine BT52 1SA, Northern Ireland, United Kingdom

ARTICLE INFO ABSTRACT

Research highlights:

> Storm-induced megarips exert a major influence on beach erosion.

> Megarip impact is persistent and cumulative during storm-groups.

> Megarips can persist for several months enhancing beach erosion and reducing beach recovery ability.

Extreme erosion on high-energy embayed beaches: influence of megarips and storm grouping

Carlos Loureiro[a,1], Óscar Ferreira[a] and J. Andrew G. Cooper[b]

[a] CIMA - Centre for Marine and Environmental Research, Universidade do Algarve, Campus de Gambelas, Edifício 7, 8005-139 Faro, Portugal
cloureiro@ualg.pt; oferreir@ualg.pt

[b] Centre for Coastal and Marine Research, School of Environmental Sciences, University of Ulster, Cromore Road, Coleraine BT52 1SA, Northern Ireland
jag.cooper@ulster.ac.uk

[1] Corresponding author: CIMA - Centre for Marine and Environmental Research, Universidade do Algarve, Campus de Gambelas, Edifício 7, 8005-139 Faro, Portugal, Telephone: +351 289800900 (ext: 7885), Fax: +351 289800969, Email: cloureiro@ualg.pt

Abstract

Megarips have long been recognized as an important, yet poorly documented, mechanism of beach erosion on high-energy embayed beaches. The persistence and cumulative effect of megarips during storm groups, are described from three embayed beaches (Arrifana, Mt. Clérigo and Amoreira) exposed to high-energy wave conditions in the mesotidal, bedrock-dominated southwestern coast of Portugal. Morphological changes, determined by topographic monitoring and supplemented by interpretation of digital imagery over two years, revealed the development of storm-induced megarips, which exerted a major influence on beach erosion. Differences in megarip influence within and between beaches are related to embayment geometry and orientation, which significantly influence the nearshore wave field. Rip location is topographically controlled, being determined by alongshore variations in breaking wave height and obliquity, along with interaction of wave-driven circulation patterns

and embayment nearshore topography. Moderate beach sand loss during individual storms was linked to the development of megarips with associated rip-neck and feeder channels. Extreme erosion, however, occurred when megarips and feeder channels persisted during successive storms, promoting continued erosion and seaward sediment export. Observations show that once initiated, megarip channels persist for several months and continue to act as conduits for offshore sediment transport under non-storm conditions. The maintenance of such rip circulation systems, driven by morphodynamic feedback, reduces beach recovery ability until the rip-neck and feeder channels are infilled.

Keywords: embayed beaches, megarips, storm groups, beach morphology, wave modelling, Portugal

1. Introduction

Severe erosion on embayed beaches has long been associated with the occurrence of large scale rip currents, or megarips (Short, 1985). Megarips occur when the embayment topography, particularly around headlands, alters surf zone dynamics during high waves, inducing persistent longshore gradients and the development of cellular circulation (Short and Masselink, 1999). Due to high offshore flow velocities and the seaward extent of megarips (beyond the surf zone), sediment is removed from the beach and transported seaward, to the lower shoreface or even the inner shelf (Short, 1985; Short and Masselink, 1999; Short, 2010).

The influence of embayed beach configuration in the location and dynamics of large scale rip currents was presented early in the rip current literature by McKenzie (1958). However, recent advances in understanding of rip current flow kinematics and morphological coupling have been based on rip channelled beaches on open coastlines, rather than topographic rips

55 and megarips (MacMahan et al., 2006, 2010). Apart from the first records of megarip flow on
56 the nearshore by Evans et al. (2000) and Coutts-Smith (2004), no other measurements of
57 megarip flow have yet been made in the beach or surfzone. The highly dynamic and energetic
58 conditions associated with the occurrence of megarips make instrument deployment
59 hazardous, and have constrained attempts to measure megarip dynamics. Nevertheless,
60 megarips have been associated with extreme beach and even foredune erosion during major
61 storm events along high-energy embayed coastlines (e.g. Thom, 1974; Short and Hesp, 1982),
62 and offshore sediment transport from beaches (e.g. Coutts-Smith, 2004; Smith et al., 2010).
63 On unconstrained sandy beaches, severe erosion is traditionally associated with extreme
64 single storms. However, the occurrence of storm groups has become a focus of renewed
65 attention, since the combined erosion of successive storms can be similar or even higher than
66 a single storm of higher magnitude (Lee et al., 1998; Ferreira, 2005, 2006; Callaghan et al.,
67 2008). High-energy embayed beaches exposed to energetic swell and storms are considered to
68 be attuned to high-energy conditions and, therefore, require extreme events to cause
69 significant morphological change (Cooper et al., 2004). However, the morphological impacts
70 of such extreme events on embayed beaches, particularly storm groups, remain little studied,
71 except for the early report of Thom (1974). Consequently, the cumulative effects of
72 successive high-energy events on morphodynamic responses in embayed beaches (e.g. beach
73 rotation, megarip development and headland sand bypassing) are still poorly understood.
74 This paper presents observations of morphological change, obtained during frequent surveys
75 on three sandy embayed beaches in the southwestern coast of Portugal, exposed to high-
76 energy wave conditions in a mesotidal environment. Wave data was obtained for an offshore
77 location and propagated to the nearshore using numerical wave modelling, in order to
78 investigate the morphological response to wave forcing. Previous work (Loureiro et al., 2011)
79 has indicated that the general pattern of seasonal change along the study sites is disturbed by

storm-group action which induces dramatic beach erosion, and that beach response is not uniform alongshore.

The overall aim of this paper is to examine the role of megarips and storm grouping in the extreme erosion observed in embayed beaches exposed to high-energy wave conditions. The specific objectives are to: (i) quantify the volumetric and morphological beach response to wave forcing, particularly focusing on the impact of storm groups and the development of rip current systems; (ii) analyse the conditions for megarip development in the three beaches based on morphodynamic behaviour parameters and numerical wave modelling; and (iii) evaluate the role of storm grouping in the persistence and enhanced action of megarips and discuss the impacts on extreme erosion and recovery ability of embayed beaches.

2. Environmental setting

Along the bedrock-dominated southwestern coast of Portugal, beaches occur generally in embayments associated with small streams or in coastal re-entrants within the Carboniferous shale and greywacke cliffs. The coast is directly exposed to the North Atlantic swell, experiencing mean offshore significant wave heights (H_{so}) between 1.5 and 2 m and peak periods (T_p) between 9 and 13 s, predominantly from northwest to westerly directions (θ) (Fig. 1) (Costa et al., 2001; Costa and Esteves, 2010). Energetic wave conditions are relatively frequent, with H_{so} exceeding 3 m 10% of the time (Costa et al., 2001). Storms along the western Portuguese coast are associated with $H_{so} \geq 5$ m (Pita and Santos, 1989), and are generally caused by frontal systems connected with high to mid-latitude depressions crossing the North Atlantic (Costa et al., 2001). Storm groups occur frequently on the west coast of Portugal, once every year for a group of two storms and once every four years for a group of three storms (Ferreira, 2005). Storm groups may also be associated with the landfall of frontal systems. Their occurrence is related to a southerly position of the Azores High Pressure

105 System, which allows successive depressions to follow a more southerly path and impact
106 directly on the Portuguese coast. Individual storms with high waves usually last an average of
107 two days, but occasionally they can persist for more than five days (Costa et al., 2001; Costa
108 and Esteves, 2010).
109 Tides along the south-western coast of Portugal are semidiurnal and mesotidal, with
110 maximum spring tidal range of 3.6 m and maximum tidal elevation about 2 m above mean sea
111 level (MSL).
112
113 **Figure 1**
114
115 Field surveys were conducted in Arrifana, Mt. Clérigo Amoreira and beaches (Fig. 1), the
116 former two directly exposed to the dominant north-westerly waves while Arrifana roughly
117 faces west and is partially protected by a prominent northern headland. All three beaches are
118 composed of well-sorted, medium sand and, being exposed to a high-energy wave climate, are
119 modally dissipative or intermediate skewed to dissipative in state. Arrifana is a swash-aligned
120 beach, completely enclosed by up to 100 m-high cliffs, and separated from them by coarse
121 gravel and boulders deposit. The subaerial beach is narrow, rarely presenting a well defined
122 berm, while the intertidal area is wide and flat and frequently featureless. A wide and flat
123 intertidal area also characterizes Mt. Clérigo, yet the subaerial beach is wide and backed by
124 partly vegetated dunes in the south and centre, while the northern sector is narrow and backed
125 by 50 m-high cliffs. Amoreira beach is wide and backed by an extensive dune field. This
126 embayment contains a bay-barrier estuary, with a small tidal stream. The beach has a
127 persistent low tide terrace that is occasionally crossed by a migrating tidal channel. This
128 creates a ridge and runnel-like morphology and produces a recurring planform rotation of

Amoreira beach that is driven by the interaction of fluvial discharge and oceanographic forcing (Freire et al., 2011).

3. Methods

3.1. Beach and nearshore morphology

Morphological surveys were conducted in Arrifana, Mt. Clérigo and Amoreira beaches along cross-shore beach profiles over a two year period, between September 2007 and September 2009. Surveys were undertaken regularly every two months, and were complemented by event-driven surveys performed immediately after storms and 15 to 30 days later to monitor beach recovery, totalling 20 surveys completed on each beach over the two year period. Three profiles representative of the different beach sectors and with alongshore profile spacing between 200 and 100 m (Fig. 1), were monitored on each beach using a Trimble RTK-GNSS (Real Time Kinematic Global Navigation Satellite System). Surveys were always performed at low tide, preferentially during spring tides, and extended from the frontal dune or cliff base to waning depths, at least up to the mean low water spring level (MLWS), 1.4 m below mean sea level (MSL), or further seaward.

Volumetric change was computed for each profile (in m^3 per unit metre of beach length) by integrating the beach profile above the MLWS level. Recognition of a nodal point at approximately the MLWS level, separating berm and subtidal terrace changes on an exposed beach in Southern Portugal by Almeida et al. (2011), suggests a vertical morphodynamic separation of the profile at this level and, therefore, renders it as an appropriate lower level for beach volume calculation. Net gain or loss of sediment over the MLWS level is then considered an indicator of cross-shore exchange of sediment between (i) the subaerial and intertidal beach and (ii) the subtidal beach.

153 Detailed topo-bathymetric surveys of the all three beaches and nearshore areas were
154 performed in September 2008, during a period of general beach accretion, using a boat-
155 mounted single beam echosounder, RTK-GNSS positioning and tidal correction. Survey lines,
156 spaced at 100 to 150 m intervals, extended seaward from the beach between 1 and 2 km,
157 reaching depths of approximately 30 m bellow MSL. Prior to grid interpolation, raw survey
158 data was smoothed using a moving average with a 50 m window, considered suitable to
159 resolve nearshore sandbars at the study area. After smoothing, the bathymetric grids were
160 produced using a locally adapted spline interpolation, which retained the general smoothness
161 of the nearshore area, but also allowed for sharp changes along submerged rocky outcrops to
162 be represented.
163
164 *3.2. Rip and feeder configuration*
165 Recent studies of rip systems at mesocale (months to years) have been based in visual
166 identification of rip channels, mostly using video imaging techniques (e.g. Ranasinghe et al.,
167 2004; Holman et al., 2006; Turner et al., 2007; Orzech et al., 2010, Gallop et al., 2011).
168 However, on the majority of cases, these are subjective methods based on manual visual
169 analysis (Gallop et al., 2011), and have been particularly noted to be of limited use in
170 energetic conditions, when megarips develop (Short, 1985), as large waves break across the
171 entire surfzone, hampering the identification of rip channels (Orzech et al., 2010; Gallop et
172 al., 2011). Repeated bathymetric surveys have been also used to characterize rip morphology,
173 but only during short-term field experiments covering restricted areas (e.g. MacMahan et al.,
174 2005) due to the logistical difficulties involved in monitoring the surfzone and nearshore in
175 dynamic and energetic environments where rip currents develop (Brander et al., 2001).
176 In the present work, a combined analysis of visual evidence and morphological patterns,
177 synthesized in Fig. 2, is used to identify rip-neck and feeder channels and assess their

178 interaction with beach profiles, in an attempt to overcome the shortcomings identified above.
179 Shallow nearshore bars and rip channels along the shoreline and surfzone are relatively easy
180 to identify visually (Holman et al., 2006; Thornton et al., 2007; Turner et al., 2007). Increased
181 turbulence due to wave-current interactions, gaps in the breaking line, streaks of darker water
182 and foam patches seaward of the breakers are distinctive features that make rip identification
183 straightforward (Aagaard and Masselink, 1999). Instantaneous snapshot images were obtained
184 during field surveys with a standard digital camera from high-ground fixed positions in each
185 embayment, located in Fig. 1. Due to the narrow field of view of the camera used, several
186 images were obtained sequentially with significant overlap and, when possible, mosaiced
187 automatically using AutoStitch© (Brown and Lowe, 2007) to produce panoramic images of
188 the entire embayments. The images were always acquired during low tide as the
189 morphological expression of rip and feeder channels is amplified at this tidal stage (Brander,
190 1999). These were then used to identify rip and feeder channels and their locations relative to
191 surveyed sections of the beach. Visual signatures of rip systems around the lower intertidal
192 and shallow subtidal areas were characterized in accordance with a subjective boundary
193 description, similar to the approach used by Brander et al. (2001). Fundamentally, incised
194 channels and areas of reduced wave breaking were characterized as rip systems (Turner et al.,
195 2007), while areas of intense wave breaking are associated with bars or shoals (Thornton et al,
196 2007). Rip systems were further divided into feeder and rip-neck channels according to the
197 orientation of the channels. Feeder channels are generally incised alongshore or slightly
198 obliquely, while rip-neck channels are distinctively cross-shore oriented, although not
199 necessarily perpendicular to the shoreline or wave approach.
200 Besides the visual interpretation, rip and feeder channel influence on profile morphology was
201 analysed according to patterns of morphological relief described by Brander and Cowell
202 (2003). Rip-neck channel morphology presents sharply inflected slopes, with abrupt

deepening (Fig. 2), that gradually become shallower in the offshore direction (Brander and Short, 2000; Brander and Cowell, 2003). Moreover, the bottom of rip channels frequently contain coarse mega-ripples (Cook, 1970), that reflect the intense sediment transport. Feeders are morphologically distinguishable by being generally alongshore-oriented (some obliquity may be present), and also because the cross-shore profile along a feeder channel generally presents a marked trough followed seaward by bar morphology (Fig. 2) (Brander and Short, 2000; Brander and Cowell, 2003; Bruneau et al., 2009).

Further indications of rip-neck and feeder channels were recorded during the surveys, performed during low tide when rip flows are higher due to tidal modulation (Brander and Short, 2000; MacMahan et al., 2006). Distinctive and strong longshore and offshore flows that could be felt while undertaking topographic surveys further enhanced recognition of feeder and rip-neck influence whenever the profiles were immediately adjacent to such channels (within a distance of approximately 20 m).

Following the analysis of visual evidence and morphological patterns, along with the auxiliary indications of nearshore flows, rip-neck and feeder interaction with beach topographic profiles was classified according to three situations outlined in Fig. 2: a) profile intersected by, or immediately fronting a rip-neck channel; b) profile intersected or immediately adjacent to a feeder channel; c) profile without immediate influence of rip-neck or feeder channel. Although surveys were not performed *during* high-energy events but immediately after, the megarips and associated feeder channels remain as distinctive features for a significant time, as strong rip flows persist even under subsequent moderate waves (Short, 1985) and significant time is needed for morphological readjustment (McKenzie, 1958). This is particularly noticeable for rips that are topographically controlled by headlands (Gallop et al., 2011).

228 **Figure 2**

229

230 *3.3. Offshore wave data*

231 Offshore wave data were recorded by a Datawell directional wave buoy located at Sines (Fig.
232 3), 65 km north of the study areas in a mean water depth of 97 m. The data, composed of
233 significant wave height, peak period and peak wave direction, were obtained from Instituto
234 Hidrográfico. Gaps in the measured wave record (~20% of the total record) were filled using
235 modelled data from WANA network deepwater grid point 1044052 (Fig. 3) (Lahoz and
236 Albiach, 2005), since significant correlation was obtained for wave height ($\rho \leq 0.001$, $n =$
237 6137, $R = 0.88$) and peak period ($\rho \leq 0.001$, $n = 6137$, $R = 0.61$). Correlation analysis was also
238 performed for the several WANA grid points along the south-western coast of Portugal to
239 evaluate if waves at Sines were representative of the deepwater conditions further south, in
240 locations closer to the study area (Fig. 3). The analysis provided highly significant correlation
241 between all WANA grid points for both H_{so} and T_p ($\rho \leq 0.001$, $n = 8276$, $R \geq 0.92$), suggesting
242 close similarity of wave conditions along the south-western Portuguese coast.

243

244 **Figure 3**

245

246 *3.4. Nearshore wave propagation*

247 Numerical wave modelling with SWAN (Simulating WAves Nearshore; Booij et al., 1999)
248 was used to explore nearshore wave conditions for moderate and high-energy conditions.
249 SWAN is an Eulerian, phase averaged, third-generation wave model that simulates the
250 refractive propagation and evolution of the wave spectrum, and has been shown to accurately
251 reproduce the nearshore wave field over complex bathymetries (e.g. Long and Özkan-Haller,
252 2005; Gorrel et al., 2011).

253 SWAN was run in stationary mode, *i.e*. time is removed from the formulations and waves are
254 assumed to propagate instantaneously across the modelling domain, using a nested scheme
255 composed of three regular grids (Fig. 4). Grid resolutions of 100, 20 and 10 m were chosen
256 for the large, medium and smaller grids, respectively. Model predictions were initialized on
257 the three open boundaries of the larger grid with the parametric input from the wave buoy
258 time series, using a JONSWAP spectral shape to represent the wave field. Input boundary
259 conditions for the medium and small grids were determined from the computations over the
260 large and medium grids, respectively. SWAN simulations accounted for non-linear triad
261 wave-wave interactions, as they are rather important in shallow coastal areas (Booij et al.,
262 1999), for bottom friction dissipation using the default variable JONSWAP expression
263 according to Hasselmann et al. (1973) and for breaking dissipation according to the default
264 bore-based model of Battjes and Jansen (1978). A depth-induced wave breaking parameter (γ)
265 of 0.78 was chosen, as this is a commonly accepted value of γ (Ranasinghe et al., 2004), and
266 was verified by dedicated tests on SWAN performance by Wood et al. (2001).
267 The nearshore wave field was computed for a range of offshore wave conditions, representing
268 an increase from moderate to high-energy waves according to classes of 0.5 m from $H_{so} \geq 0.5$
269 m to $H_{so} \geq 7$ m. Taking into consideration the importance of storm events, different storm
270 conditions were modelled independently. Average offshore conditions for a WNW, W and
271 WSW storm were propagated into each embayment to investigate the combined effects of
272 nearshore bathymetry and wave direction in the wave field using realistic conditions, while
273 synthetic storms scenarios with constant H_{so} and T_p of 5 m and 15 s, respectively, but variable
274 offshore wave directions (NW, W and SW), were used to isolate the effect of incoming wave
275 direction. Mean conditions during the January-February 2009 storm group were also modelled
276 independently for each embayment. Breaking wave heights were obtained for 10 m bins
277 alongshore for each embayment by determining the location where wave dissipation due to

278 depth induced breaking becomes significant, defined as the most offshore location where a
279 value of 1% of depth-induced breaking is reached (Harley et al., 2007).
280
281 **Figure 4**
282
283 *3.5. Embayment scaling parameter (δ')*
284 Circulation patterns on embayed beaches were analysed parametrically using the embayment
285 scaling parameter (δ') of Short (1999), which relates the embayment configuration to the
286 incident breaking wave conditions according to Eq. (1).
287 $$\delta' = S^2 / 100 C_l H_b \quad (1)$$
288 where S is the embayment shoreline length, C_l is the embayment width (distance between
289 headlands), and H_b is the breaking wave height. This empirical approximation was derived
290 from unpublished work by Martens and collaborators on morphometric analysis of embayed
291 beaches, and presented by Short (1996) and Short and Masselink (1999). The selection of this
292 formula was based on the findings of Short (1999; 2010), who indicated that the degree of
293 headland impact on surf zone circulation and, consequently, circulation type in embayed
294 beaches can be predicted using δ'. When $\delta' > 19$, the impact of headlands is limited and
295 normal surfzone circulation operates along the embayment, similar to what would be expected
296 for unconstrained sandy beaches. As δ' ranges between 19 and 8, transitional circulation
297 prevails with headlands increasingly influencing surfzone circulation. Rip currents increase in
298 size and reduce in number and become progressively topographically-controlled. Fully
299 cellular circulation develops when $\delta' < 8$, and topography controls the surfzone circulation,
300 dominated by strong longshore flows that feed on one to two megarips draining the entire
301 embayment (Short, 1999; 2010). Following Short (1999, 2010), calculations of δ' were
302 performed considering a typical surfzone gradient of 0.01 for each embayment. This is

303 considered representative of dissipative environments such as those in this study. Values of
304 H_b were obtained from alongshore averaged SWAN simulation results and the embayment
305 configuration parameters S and C_l were obtained from GIS-based digital orthophotography
306 analysis.
307
308 **4. Results**
309 *4.1. Wave conditions*
310 High-energy events were concentrated between October and April, while during the
311 remaining months wave conditions were less energetic, although H_{so} frequently exceeded 2 m
312 (Fig. 5). Storm waves were mostly from WNW-NW directions, reflecting the storm climate of
313 the southwestern coast of Portugal (82% of storms between 1988 and 2008 were from a
314 WNW-NW direction (Costa and Esteves, 2010)). There were, however, two occasions when
315 WSW storm waves impacted the coast (April 2008 and February 2009). This occurred for
316 only a few hours, and was followed immediately by WNW waves that obliterated the effects
317 of WSW storm waves on the beaches.
318
319 **Figure 5**
320
321 Grouping of high-energy events was frequent, even though the storm threshold (H_{so} > 5 m)
322 was not reached in every single event (e.g. April 2008). If lower storm thresholds were
323 considered, such as those proposed by Costa et al. (2001) (H_{so} > 4.5 m) or Costa and Esteves
324 (2010) (H_{so} > 3.5 m for at least 12 hours with maximum H_{so} reaching 4.5 m), more high-
325 energy events would be classified as storms and storm groups. Nevertheless, the most
326 significant events during the monitoring period (dark grey in Fig. 5) were a single storm in
327 early January 2008, with H_{so} reaching 8 m and wave heights in excess of 5 m for 36 hours,

and a group of 5 consecutive storms between mid January and early February 2009. This storm group, with storm peaks in the 16th, 20th and 25th January and 01st and 05th of February 2009, represented a period of continuously high waves for 22 days with maximum H_{so} of 6.7 m. Averaged over the entire storm group duration, H_{so} was 4.5 m and T_p 14.5 s from a west-northwesterly direction (300º).

4.2. Morphological change

Time series of profile volume above MLWS level are presented in combination with the classification of rip system interaction with the cross-shore beach profiles for each embayment (Fig. 6 to 8).

4.2.1. Arrifana

At Arrifana erosion-dominated periods occurred during high waves, and were associated with the development of feeder and rip-neck channels intersecting or in the vicinity of the profiles (Fig. 6). From late November to early December 2007, following an increase in wave heights with grouping of high-energy events, average profile erosion of 27 m^3/m occurred, with the development of feeder channels adjacent to Arrifana north and south profiles. With the onset of the early January 2008 extreme storm, a further 62 m^3/m where eroded on average in Arrifana beach profiles by mid January 2008. This was accompanied by the development of rip systems in the extremities of the beach, with feeder channels intersecting both the central and southern profiles (while a rip was present in the northern section of the beach, it was located more than 20 m north of the profile location). The storm induced erosion was followed by gradual beach recovery, although without complete infilling of the rip systems. Alongshore migration of the southern rip-neck channel, which had already intersected the south profile by the time of the March 2008 survey, was associated with beach accretion, as

353 this rip was already significantly infilled. The recovery process was interrupted in mid-April
354 by a group of two storms, which reactivated the erosional conditions in the southern rip
355 system and promoted the development of another rip system in the northern section of the
356 beach. Significant recovery took place during the following months at Arrifana beach, as the
357 rip-neck and feeder channels become infilled, allowing onshore displacement of sand from
358 the intertidal to the subaerial beach.
359 Erosive conditions resumed by December 2008, with development of rip system circulation
360 across the entire embayment. It was, however, with the onset of the January-February 2009
361 storm group that most abrupt changes occurred, with generalized erosion at Arrifana beach,
362 particularly noticeable on the north and south profiles. Erosion of 117 m^3/m and 98 m^3/m in
363 the north and south profiles, respectively, was associated with the development of rip-neck
364 channels intersecting profile location, while at the central profile the development of a feeder
365 channel resulted in moderate erosion (20 m^3/m). Although all profiles at Arrifana recovered
366 significantly during the 7 months following the January-February 2009 storm group (Fig. 6),
367 it was mostly after the rip-neck and feeder channels become infilled under lower waves that
368 volumetric change increased substantially.
369
370 **Figure 6**
371
372 4.2.2. Mt. Clérigo
373 During the first year of monitoring, beach profiles at Mt.Clérigo showed similar variation to
374 that of Arrifana. Erosion dominated the period between late November 2007 and April 2008,
375 followed by accretion until mid-November 2008 (Fig. 7). During the erosion-dominated
376 period, the lowest volumes attained in the northern and central profiles, in April and March
377 2008, respectively, were associated with the development of a large-scale rip system, whose

rip-neck channel was initially located in the centre of the beach and then migrated northwards. Although no rip-neck or feeder channel could be identified adjacent to the southern profile (Fig. 7), erosion at Mt. Clérigo during the first year of monitoring reached its maximum in this profile with the removal of 122 m^3/m of sediment in relation to the initial profile volume. Between November 2008 and early April 2009, a second erosion-dominated period associated with high waves and storm grouping resulted in extreme erosion throughout the entire Mt. Clérigo embayment. Average erosion of 98 m^3/m for Mt. Clérigo beach profiles marked the initial phase of this erosion-dominated period, which lasted until early January 2009. During this initial phase no rip-neck or feeder channels developed in the vicinity of the south profile, while feeder channels interacted with the centre and north profiles. The second phase of erosion, between early January and early April 2009, occurred in close association with the January-February 2009 storm group (Fig. 7). On average, this second phase led to a further 196 m^3/m of sand being removed from the profiles, with most of the erosion concentrated during the storm group (average erosion of 167 m^3/m between 11/01/2009 and 09/02/2009). The extreme erosion during the storm group was accompanied by the development of a wide megarip in the centre of the beach, with a rip-neck channel intersecting the lower intertidal section of the central profile. Connected to it, feeder channels from both sides of the beach intersected the southern and northern profiles. Beach recovery was initiated in late April for all three profiles but even after 5 months the volume restored to the beach was significantly lower than what was removed between November 2008 and early April 2009 (on average recovery only reached 21% of the eroded volume). Notably, during the recovery period, the central rip-neck channel and the northern feeder channel were still active, hindering significant recovery, while sediment accretion on the southern profile was only initiated after April 2009, once the feeder channel had been infilled (Fig. 7).

403 **Figure 7**

404

405 4.2.3. Amoreira

406 Beach profile response to high-energy events at Amoreira beach was variable during the first
407 year of monitoring, although the association between rip-neck or feeder channels and erosion-
408 dominated periods was still clearly recognized (Fig. 8). Significant erosion on central and
409 southern profiles occurred immediately in response to December 2007 energetic waves group
410 (three events with H_{so} around 4 m in 15 days), and the early January 2008 extreme storm. This
411 later erosional event was accompanied by the development of a rip system with feeder
412 channels interacting with the central and southern profiles. Eroded volumes reached 148 m^3/m
413 in the southern profile and 110 m^3/m in the central profile, but only 13 m^3/m in the northern
414 profile. However, following a northward displacement of the rip system in the subsequent
415 months, 213 m^3/m of sand were removed from the north profile. Recovery from this erosive
416 period took as much as 7 to 9 months, although it did not proceed linearly in the central and
417 southern profiles, occurring subsequent to the infilling of rip-neck and feeder channels. Under
418 the action of the January-February 2009 storm group, severe erosion occurred in the northern
419 and central profiles (Fig. 8), while the south profile only experienced moderate erosion.
420 Maximum erosion of 268 m^3/m was registered in the central profile, closely followed by the
421 northern profile with an eroded volume of 243 m^3/m. During this storm group a wide megarip
422 developed in the centre of the beach, with a rip-neck channel intersecting the central profile.
423 This was directly connected to a deep feeder channel in the northern section. Both features
424 persisted for several months, hindering beach recovery in the northern and central profiles
425 (Fig. 8).

426

427 **Figure 8**

428

429 *4.3. Nearshore wave modelling*

430 In the absence of hydrodynamic measurements in the shoaling and surfzone of the three
431 embayments studied, particularly during moderate and high-energy events that drive most
432 significant morphological changes, numerical wave modelling was used for simulation of
433 nearshore wave field. Breaking wave heights were obtained for increasing offshore wave
434 conditions (Table 1), real and synthetic storms (Table 2 and Fig. 9) and also for the average
435 conditions during the January-February 2009 storm group (Fig. 10).

436

437 **Table 1**

438

439 **Table 2**

440

441 Model results highlight the sensitivity of the alongshore variation in nearshore wave heights
442 to the offshore bathymetry in Arrifana embayment, while Mt. Clérigo and Amoreira present
443 fairly alongshore uniform conditions. Modelled breaking wave heights indicate that for Mt.
444 Clérigo and Amoreira beaches, which are directly exposed to the dominant north-westerly
445 waves, alongshore variation in breaking wave height is almost negligible, as evidenced for
446 standard deviation values below 0.1 in all simulations (Table 1). On these two beaches,
447 breaking wave height is on average equivalent to the offshore wave height, with most
448 variation within a difference range of 10%. Arrifana beach, conversely, shows considerable
449 alongshore variation and important reductions in breaking wave height comparing to the
450 offshore counterpart (Fig. 9 and Table 1). The northern section of the beach experiences
451 breaker heights up to 3.5 m lower than the southern section, during the most extreme
452 conditions when $H_{so} \geq 7$ m. This alongshore gradient, which increases concurrently to

offshore wave height as evidenced by increasing standard deviation values (Table 1), is due to the sheltering effect of the prominent northern headland, which forces the diffraction of the dominant west-northwesterly waves. Wave diffraction, together with refraction and attenuation on a gentle shoreface (average *tanβ* of 0.02), induces breaking wave heights on average 35% lower than the offshore wave height, but ranging between 60% and 20% lower on the northern and southern sectors, respectively.

Figure 9

The nearshore wave conditions during storms, both the observed and synthetic events (Fig. 9 and Fig. 10), reflect, in general, the alongshore gradients identified in Arrifana embayment, while highlighting higher sensitivity of Mt. Clérigo and Amoreira embayments to changes in incoming wave direction. For synthetic storms, where only wave direction has been modified, Arrifana embayment maintains significant alongshore gradients, but these are quite insensitive to the variation in wave direction, with the centre of the embayment presenting similar conditions for NW, W and SW storms (Fig. 9). Considering both the real storms (Table 2) and synthetic storms, breaking wave conditions calculated for Mt. Clérigo and Amoreira embayments are similar, not only in height, but also alongshore uniformity (Fig. 9 and Fig. 10). In these two embayments offshore regular bathymetry precludes noticeable alongshore variations, but their orientation does enhance the attenuation of real WSW and synthetic SW stormy waves, with modelled breaking wave heights being reduced by up to 1.5 m.

Figure 10

478 *4.4. Embayment circulation*

479 Parametric analysis of embayment circulation was performed for the modal wave conditions
480 and also for the range of modelled breaking wave heights presented in Table 1, using the
481 formulation for the embayment scaling parameter (δ') described in Eq. (1). The computed
482 values of δ' place Arrifana as an embayment modally subjected to normal circulation, owing
483 to significant length and moderate breaking wave heights (Table 3). Computing δ' for the
484 range of alongshore averaged modelled breaking wave heights in Arrifana, the wave-driven
485 circulation becomes transitional as H_b approaches 2 m, and cellular circulation is established
486 when H_b overcomes 3.5 m (Fig. 11).

487

488 **Table 3**

489

490 **Figure 11**

491

492 Mt. Clérigo and Amoreira embayments evidence similar wave conditions, as presented in the
493 nearshore wave modelling (Section 4.3), and the geometric characteristics of these two
494 embayments are also similar, as both have reduced widths and lengths. Therefore, the
495 combination of small dimensions along with similar exposure to more energetic conditions
496 renders both beaches modally cellular (Table 3). Transitional circulation is approached in
497 both embayments when H_b reduces to values below 1.5 m (Fig. 11), while normal circulation
498 occurs very infrequently ($H_b < 0.5$ m). Although a δ' value of 7 places Mt. Clérigo and
499 Amoreira embayments in a modally cellular circulation type, such a value is very close to the
500 threshold for transitional circulation (defined as $\delta' \geq 8$), implying that sustained conditions of
501 cellular circulation in both embayments are only established once H_b exceeds 2 m (Fig. 11).

502

5. Discussion

5.1. Megarips or large rips?

The results presented in this study highlight the role of megarips in the periodic erosion of sand from high-energy embayed beaches, providing new insights into their cumulative action during and after storm groups. While significant progress has been made recently in the study of the hydrodynamics and morphodynamic coupling of rip systems, particularly by field experiments (e.g. Brander and Short, 2000; MacMahan et al., 2005; Bruneau et al., 2009; Austin et al., 2010), such efforts have concentrated on open coast rips. Conceptually, despite their large dimensions and association with moderate to high wave conditions, those are large-scale accretionary rips associated with downstate transitions in intermediate beaches and are consequently quite different to topographic rips or megarips (Brander and Short, 2000; Short, 2007; MacMahan et al., 2010). The rip systems described here differ from such large-scale accretion rips because they develop during high-energy events (Fig. 12), when the beaches would otherwise have transitioned upstate to dissipative conditions, characterized by the absence of rip circulation (Wright and Short, 1984). Their location and development is also controlled by embayment configuration, which places then conceptually as topographic rips, transitioning to megarips under high-energy conditions and dominating the circulation of entire embayments (Short, 2010).

Figure 12

The reduced dimension of the embayments studied, combined with exposure to an energetic wave climate, contributes to circulation types influenced by embayment topography almost permanently, as indicated by the embayment scaling parameter (δ'). Despite conditions for transitional or cellular circulation may be maintained for most of the wave conditions

528 encountered in Arrifana, Mt. Clérigo and Amoreira, the actual transition for megarip
529 circulation only occurs during high waves. A breaking wave height (H_b) of 3 m was proposed
530 by Short (1985, 2010) as a threshold for the transition to megarip circulation, considering that
531 when H_b exceeds this value fully dissipative conditions would prevail (Wright and Short,
532 1984). While detailed validation of this threshold cannot be presented, analysis of the
533 variation of δ' for increasing wave heights (Fig. 11), suggests that when H_b reaches 3.5 m
534 conditions for cellular circulation are established for all embayments. The beaches studied are
535 modally intermediate to dissipative in state, and observations confirm that as H_b increases to
536 more than 3 m dissipative surfzones prevail, with megarips dominating the surfzone
537 circulation in Arrifana, Mt. Clérigo and Amoreira. When wave conditions decrease, these rip
538 systems do not cease functioning. They, however, maintain roughly the same position, not
539 experiencing significant alongshore migration as observed for accretionary/erosional rips (e.g.
540 Holman et al., 2006; Turner et al., 2007; Orzech et al., 2010). This occurs because they
541 remain topographically controlled, downgrading from megarips to large-scale topographic
542 rips.
543
544 *5.2. Megarip development*
545 Temporal and spatial changes in wave breaking drive variations in wave set-up/down,
546 producing pressure gradients that induce water-flow from areas of high waves towards areas
547 of low waves, where flow convergence creates a constrained jet-like flow that exits the surf
548 zone as a rip current (Bowen, 1969; MacMahan et al., 2006; Dalrymple et al., 2011).
549 Topographic rips and megarips share this same forcing mechanism, but while most rips are
550 driven by longshore variations in wave height due to bathymetric variation generally
551 associated with rhythmic shoals and channels in intermediate beaches (Aagaard and
552 Masselink, 1999), and less frequently with wave-wave interactions (MacMahan et al., 2006),

553 topographic rips and megarips result from longshore variations in wave height due to
554 attenuation and refraction around offshore topographic features like headlands and reefs
555 (Short, 1985).
556 Alongshore variations in breaking wave height assessed using numerical wave modelling for
557 Arrifana beach are consistent with the development of a megarip in the more protected
558 northern sector (Fig. 13). The sheltering effect of the northern headland creates a geometric
559 shadow, leading to an area of significantly lower breakers on the northern sector (Fig. 10),
560 inducing an alongshore flow towards the northern headland. The position of this megarip
561 endorses the suggestion that under extreme conditions with oblique incident waves, a wave
562 setup-driven mechanism would be responsible for the development of a megarip in the
563 protected end of an embayment (Coutts-Smith, 2004), similar to re-circulation cells present in
564 the lee of groynes, as recently demonstrated by Pattiaratchi et al. (2009). Due to nearshore
565 bathymetry and convergence of breaking waves with the circulation cell, the northern megarip
566 is deflected obliquely towards the centre of the embayment, instead of flowing straight
567 offshore. It then develops an alongshore component, visible in the rip-head plume (Fig. 12),
568 restricting the seaward extent of the northern megarip.
569
570 **Figure 13**
571
572 Development of a second megarip in a southern location, adjacent to the southern profile at
573 Arrifana beach, cannot be derived from modelled alongshore variations in breaker height
574 alone. However, there is a tendency for megarip development adjacent to headlands (as a
575 contour current) exposed to an obliquely incident wave field (Coutts-Smith, 2004; Short,
576 2010), just as a rip system develops in the updrift side of a groyne or structure (Pattiaratchi et
577 al., 2009; Dalrymple et al., 2011). Driven by oblique waves, an alongshore current runs

parallel to the beach and is forced to turn seaward against the downdrift headland. Lateral positioning of the southern megarip at Arrifana supports this hypothesis, due to the occurrence of obliquely incident waves. Despite the reduced extension of the southern headland, the beach is bounded by submerged rocky outcrops approximately 100 m southwards of profile south, which force the alongshore current to deflect offshore, forming the distinctive southern megarip (Fig. 13). A divergence zone, separating the alongshore currents feeding both the northern and southern megarips, is located in the centre of the embayment, as evidenced by the post-storm snapshot in Fig. 12. The location of a divergence zone in the alongshore currents is associated with changes in the alongshore gradient in wave height due to topographic sheltering (Pattiaratchi et al., 2009). Breaking wave heights obtained from wave modelling confirm that the centre of Arrifana embayment evidences more constant wave conditions, with intermediate heights between the lower waves in the northern section and the higher waves in the southern section (Fig. 9).

Megarips have also been noted in the centre of longer embayments (>1-2 km), associated with shore normal incident waves (Short, 1985; Short, 2010). Although Mt. Clérigo and Amoreira are significantly shorter than this (approximately 600 m), both beaches are normally exposed to the energetic north-westerly waves. During high-energy events, one megarip developed roughly on the centre of each embayment, occasionally extending to the northern sectors of both beaches (Fig. 14 and Fig. 15). The absence of noteworthy alongshore variation in modelled breaking wave height at Mt. Clérigo and Amoreira (Fig. 9 and Fig. 10), provide no immediate explanation for megarip development due to breaker gradients at these beaches. However, development of megarips in the centre of embayed beaches has been shown to occur during storms (Wright et al., 1979; Short, 1985), and recent analytical modelling approaches by Silva et al. (2010) suggest development of cellular circulation with a rip developing in the centre of embayed beaches under normal incident waves. Such rip

603 circulation is related to embayment geometry influencing the nearshore wave field,
604 particularly breaker height and wave obliquity at breaking, as suggested by Huntley et al.
605 (1988) and confirmed numerically by Silva et al. (2010). While obtained for low to moderate
606 wave conditions, the results of Silva et al. (2010) provide a hypothesis for the initial
607 development of an embayment scale rip circulation system. Under increasing wave heights
608 this circulation system would transition into a megarip since, as suggested by the authors,
609 once the circulation is established, wave height variation would only strengthen or weaken the
610 current velocities without modifying the circulation patterns.
611 At Mt. Clérigo, nearshore topographic control is likely to also influence the development and
612 location of a megarip in the centre of the embayment, as a rocky outcrop in the lower
613 intertidal and subtidal zone extends obliquely from the south to the centre of the beach (Fig.
614 14). This outcrop provides a permanent barrier that forces longshore currents to flow seaward,
615 as reported elsewhere by Davidson-Arnott (2010), scouring a channel that widens to a large
616 megarip during high-energy events.
617
618 **Figure 14**
619
620 Apart from the Arrifana megarips, where conditions for alongshore variation in breaker height
621 inducing pressure gradients are maintained due to topographic sheltering, no other megarip
622 could be inferred from wave modelling results. All models of rip circulation are forced by
623 alongshore variations in wave height (MacMahan et al., 2006), and under homogeneous
624 alongshore contours, as observed for Amoreira and M. Clérigo embayments, such variations
625 are not expected to be significant. Nonetheless, as evidenced in previous studies, even small
626 bathymetric irregularities can influence surfzone hydrodynamics, inducing wave gradient-
627 driven rip circulations (Calvete et al., 2007; MacMahan et al., 2008; Dalrymple et al., 2011).

628

629 **Figure 15**

630

631 *5.3. Enhanced erosion by megarips and storm grouping*

632 Localized beach and dune erosion has been associated to the coupling between rhythmic
633 cuspate shorelines and rip currents in long embayments (Thornton et al., 2007). Along highly
634 compartmentalized coastlines, with small and bedrock-bounded embayed beaches, cellular
635 circulation, and particularly megarips, has also been presented as a major mechanism of beach
636 erosion (Short, 1985), while undertow has been found to be of reduced efficiency in cross-
637 shore sediment transport (Dehouck et al., 2009). Destructive effects and erosive hazards may
638 be greatly enhanced by the action of megarips (Wright, 1981), especially because of their
639 ability to transport sediment, flushing entire beach compartments through their wide and deep
640 feeder systems and intense rip flows (Short, 1979; Wright, 1981). Most severe beach erosion
641 occurs in the lee of megarips (Short, 1985), and for profiles at Arrifana south, Mt. Clérigo
642 centre and Amoreira centre, where megarip development was more frequent, erosion was
643 generally higher than in the remaining profiles. Profiles intersecting or adjacent to feeder
644 channels draining to the main rip also experienced enhanced erosion, as evidenced in profiles
645 Mt. Clérigo north and south and Amoreira north. In contrast, Amoreira southern and Arrifana
646 central profiles presented lower variation, being also less regularly associated with either rip-
647 neck or feeder channels (Fig. 6 and Fig. 8).

648 The coupling of rip-neck and feeder channels with enhanced erosion of Arrifana, Mt. Clérigo
649 and Amoreira beach profiles is noticeable during individual high-energy events, although the
650 relationship is not always immediate or linear since morphodynamic response is influenced by
651 antecedent conditions, requiring an adjustment time (Wright and Short, 1984). Nevertheless,
652 under the action of the January-February 2009 storm group the relationship is remarkable.

Storm groups, or sequences of storms without significant recovery in between (Ferreira, 2006), have long been recognized as an important mechanism for extreme erosion of embayed beaches (Thom, 1974), driving dramatic shoreline retreat on erosion hotspots (Smith et al., 2010), or triggering erosion dominated periods of several years (Thom and Hall, 1991). Considering that the most significant beach cut on short embayed beaches is produced by megarips (Wright, 1981), their maintenance during storm groups would be expected to produce extreme and continued erosion. Our results provide field evidence of this process. All profiles were influenced by megarips during the January-February 2009 storm group, either by rip-neck or feeder channels, inducing widespread beach erosion. Except for profiles Arrifana centre, located in a divergence zone where feeder channel influence was tangential, and Amoreira south where feeder influence was short-lived, all profiles were severely eroded. This storm group clearly demonstrated the spatial extent of megarips and confirmed their ability to dominate the circulation of entire embayments. Moreover, the persistence of megarip action during the storm group led to the development of large and deep rip-neck and feeder channels (Fig. 12), which required a significant post-storm period to be infilled. Rip currents remained active for a long period, as they were coupled to the underlying morphology, and caused continued erosion.

5.4. Implications for beach recovery

Seaward transport of sediment is greatly enhanced by megarips, which are considered to be responsible for sediment exchange between embayed beaches and the nearshore or even the inner-shelf (Short, 1985; Coutts-Smith, 2004). Sediment removed from the beach by megarips has been shown to be deposited at depths of 10-25 m (Coutts-Smith, 2004; Smith et al., 2010), owing to seaward extensions of approximately 1.5 to 4 times the surfzone width (Coutts-Smith, 2004; Dalrymple et al., 2011), or between 1 and 2 km (Short, 2010). Sand withdrawn

678 from Arrifana, Mt. Clérigo and Amoreira beaches by megarips was presumably transported to
679 depths between 10 to 15 m, based on schematic mapping (Fig. 13 to 15), and spread out on
680 the lower shoreface, as observed elsewhere by Coutts-Smith (2004) and Smith et al. (2010),
681 resulting in net loss of sediment from beaches. There were however, significant differences
682 between the study beaches. These can be explained by differences in wave forcing, since
683 increase in incident wave height is associated with higher rip current speeds (Pattiarachi et al,
684 2009; Dalrymple et al., 2011), and also a higher offshore extent of megarips (Coutts-Smith,
685 2004). On Mt. Clérigo and Amoreira beaches, due to normal exposure to incident storm
686 waves, which break without considerable attenuation driving either stronger or/and seaward
687 extended megarip flows, a higher volume of sand was lost and apparently to greater depths, as
688 materialized by the inability of both beaches to recover in the following months. On Arrifana
689 beach, where breaking wave heights are consistently lower, net volumetric loss was reduced,
690 although severe erosion occurred during the January-February 2009 storm group.
691 During storm groups, sediment lost from the beach and the upper shoreface is expected to be
692 even greater than for single storm events (Cowell et al., 1999), due to inability to reach a
693 storm equilibrium profile during storm groups (Inman et al., 1993) and continued conditions
694 for megarip-driven erosion as a result of coastal disequilibrium (Smith et al., 2010). While
695 megarips developed during the first year of monitoring caused moderate erosion, even with
696 the January 2008 extreme single storm, no significant net volumetric loss was observed. In
697 contrast, erosion associated with the January-February 2009 storm group was significant,
698 probably associated with substantial export of sediment to the nearshore, promoted by the
699 long duration of the event.
700 Once formed, and being topographically forced, large rips can persist in the same location for
701 extended periods (Short, 1985), evidencing a much longer lag-time in their response to
702 changing wave conditions (Gallop et al., 2011). Owing to positive morphodynamic feedback,

703 alongshore gradients are maintained and eventually enforced. Rip-neck and feeder channels
704 continue then to flush and erode sediment, resulting in stable circulation patterns which have
705 been observed to persist for several years in the case of rips controlled by headlands (Gallop
706 et al., 2011). Considerable time is then needed for readjustment after megarip-induced erosion
707 (McKenzie, 1958), and complete recovery can require several years (Wright and Short, 1983).
708 Since high-energy conditions were maintained throughout the January-February 2009 storm
709 group, megarip circulation was continuously active for at least 22 days, creating large and
710 deep channels. Consequently, rip-neck and feeder channel influence on beach profiles was not
711 only intense but also persistent. Beach recovery has been significantly inhibited, except for
712 Arrifana beach, and channel infilling has been occurring slowly, mostly due to onshore and
713 lateral expansion of subtidal and lower intertidal shoals. Once the channels become infilled a
714 faster recovery is expected, as evidenced in Arrifana beach. The enhanced ability of Arrifana
715 beach to recover after the storm group suggests that sediment taken from the beach remained
716 at shallower depths, within the constrained environment of the embayment, and was available
717 for subsequent rip and feeder channel infilling allowing beach recovery, most likely because
718 megarips at Arrifana were less intense and/or extensive.
719
720 **6. Conclusion**
721 Morphological change in three embayed beaches along the high-energy south-western coast
722 of Portugal was monitored over two years. During this period, profile erosion has been mostly
723 related to the development of megarips and associated rip-neck and feeder channels.
724 Differences within and between beaches were related to embayment geometry and
725 orientation. On short beaches normally exposed to incident storm waves (Mt. Clérigo and
726 Amoreira), a single megarip developed in the centre of each embayment, while obliquely
727 incident waves were associated with the development of two megarips in both extremities of

Arrifana embayment, driven by marked alongshore gradients in breaking wave height and interaction with embayment boundaries.

On the three embayed beaches studied, moderate erosion was observed during individual storms, and more importantly, extreme erosion occurred when megarips persisted for several weeks during the action of a storm group. Net sediment loss in the more exposed Mt. Clérigo and Amoreira beaches suggests sand export to the lower shoreface, driven by the persistent action of megarips during the storm group. While megarips have long been recognized as an important mechanism of embayed beach erosion, their continued and enhanced action during storm groups has only now been demonstrated, providing a clear connection between megarips and storm groups in the extreme erosion of embayed beaches. This study also demonstrates that the maintenance of a rip circulation pattern after storms (or storm groups), enforced by morphodynamic feedback, reduces beach recovery ability until the rip-neck and feeder channels are infilled.

Comprehensive field measurements of megarips have yet to be accomplished (e.g. including measurements of surfzone hydrodynamics and nearshore bathymetric change driven by megarips), and this study does not fill such gap. However, by relating megarip influence to profile variation and analysing modelled and parametric indications of megarip location, the present work provides new insights into the conditions that drive megarip development and the role of megarips in the erosion and recovery of embayed beaches.

Acknowledgements

We gratefully acknowledge the help of everyone involved in the fieldwork data collection, especially at dawn during cold winter stormy days. Thanks also to Rui Taborda, Guillaume Dodet and Xavier Bertin for providing initial training with SWAN, and Derek Jackson for discussion of modelling aspects. Mara Nunes and Thomas Smyth suggested improvements to

753 early versions of the manuscript. This work is a contribution to BAYBEACH project
754 (Evolution and Management of Embayed Beaches in Contrasting Environments) funded by
755 FCT under contract PTDC/CTE-GEX/66893/2006. Carlos Loureiro was supported by FCT,
756 grant reference SFRH/BD/27878/2006. Hydrodynamic data from Sines buoy were provided
757 by Instituto Hidrográfico. Modelled WANA wave data were kindly supplied by Puertos del
758 Estado.
759

760 ## References

761 Aagaard, T., Masselink, G., 1999. The surf zone. In: Short, A.D. (Ed.), Handbook of Beach
762 and Shoreface Morphodynamics. John Wiley & Sons, Chichester, pp. 71-118.
763 Almeida, L.P., Ferreira, Ó., Pacheco, A., 2011. Thresholds for morphological changes on na
764 exposed sandy beach as a function of wave height. Earth Surface Processes and
765 Landforms, 36 (4), 523-532.
766 Austin, M., Scott, T., Brown, J., Brown, J., MacMahan, J., Masselink, G., Russel, P., 2010.
767 Temporal observations of rip current circulation on a macro-tidal beach. Continental
768 Shelf Research, 30 (9), 1149-1165.
769 Battjes, J.A., Janssen, J.P.F.M., 1978. Energy loss and set-up due to breaking of random
770 waves. Proceedings of the 16th International Conference on Coastal Engineering.
771 ASCE, New York, USA, pp. 569-587.
772 Booij, N., Ris, R.C., Holthuijsen, L.H., 1999. A third-generation wave model for coastal
773 regions - 1. Model description and validation. Journal of Geophysical Research, 104
774 (C4), 7649-7666.
775 Bowen, A.J., 1969. Rip Currents 1. Theoretical Investigations. Journal of Geophysical
776 Research, 74 (23), 5467-5478.

777 Brander, R.W., 1999. Field observations on the morphodynamic evolution of a low-energy rip
778 current system. Marine Geology, 157 (3-4), 199-217.
779 Brander, R.W., Short, A.D., 2000. Morphodynamics of a large-scale rip current system at
780 Muriwai Beach, New Zealand. Marine Geology, 165 (1-4), 27-39.
781 Brander, R.W., Cowell, P.J., 2003. A trend-surface technique for discrimination of surf-zone
782 morphology: rip current channels. Earth Surface Processes and Landforms, 28 (8),
783 905-918.
784 Brander, R.W., Cowell, P.J., Short, A.D., 2001. Morphometric approaches to describing rip
785 current behaviour. Journal of Coastal Research, SI 34, 128-137.
786 Brown, M., Lowe, D., 2007. Automatic panoramic image stitching using invariant features.
787 International Journal of Computer Vision, 74 (1), 59-73.
788 Bruneau, N., Castelle, B., Bonneton, P., Pedreros, R., Almar, R., Bonneton, N., Bretle, P.,
789 Parisot, J.P., Sénéchal, N., 2009. Field observations of an evolving rip current on a
790 meso-macrotidal well-developed inner bar and rip morphology. Continental Shelf
791 Research, 29 (14), 1650-1662.
792 Callaghan, D.P., Nielsen, P., Short, A.D., Ranashinge, R., 2008. Statistical simulation of wave
793 climate and extreme beach erosion. Coastal Engineering, 55 (5), 375-390.
794 Calvete, D., Coco, G., Falqués, A., Dodd, N., 2007. (Un)predictability in rip channel systems.
795 Geophysical Research Letters, 34, L05605.
796 Cook, D.O., 1970. Occurence and geologic work of rip currents off southern California.
797 Marine Geology, 9 (3), 173-186.
798 Costa, M., Esteves, R., 2010. Clima de agitação marítima na costa oeste de Portugal
799 Continental. Proceedings of XI Jornadas Técnicas de Engenharia Naval – O Sector
800 Marítimo Português. Edições Salamandra, Lisboa, Portugal. 413-426.

801 Costa, M., Silva, R., Vitorino, J., 2001. Contribuição para o estudo do clima de agitação
802 marítima na costa Portuguesa. Proceedings of 2as Jornadas de Engenharia Costeira e
803 Portuária. AIPCN, Aveiro, Portugal, 20 p. (CD-ROM).
804 Coutts-Smith, A., 2004. The significance of mega-rips along an embayed coastline. Ph.D.
805 Thesis, University of Sydney, Australia.
806 Cowell, P.J., Hanslow, D.J., Meleo, J.F., 1999. The Shoreface. In: Short, A.D. (Ed.),
807 Handbook of Beach and Shoreface Morphodynamics. John Wiley & Sons, Chichester,
808 pp. 39-71.
809 Dalrymple, R.A., MacMahan, J.H., Reniers, A.J.H.M., Nelko, V., 2011. Rip currents. Annual
810 Review of Fluid Mechanics, 43, 551-581.
811 Davidson-Arnott, R., 2010. Introduction to Coastal Processes and Geomorphology.
812 Cambridge University Press, Cambridge.
813 Dehouck, A., Dupuis, H., Sénéchal, N., 2009. Pocket beach hydrodynamics: the example of
814 four macrotidal beaches, Brittany, France. Marine Geology, 266 (1-4), 1-17.
815 Evans, P., Hanslow, D., Coutts-Smith, A., You, Z., 2000. Nearshore-Inner Shelf Sediment
816 Exchange on the NSW Central Coast. Proceedings of the 27th International
817 Conference on Coastal Engineering. ASCE, Sydney, Australia, pp. 3151-3164.
818 Ferreira, Ó., 2005. Storm groups versus extreme single storms: predicted erosion and
819 management consequences. Journal of Coastal Research, SI 42, 221-227.
820 Ferreira, Ó., 2006. The role of storm groups in the erosion of sandy coasts. Earth Surface
821 Processes and Landforms, 31 (8), 1058-1060.
822 Freire, P., Taborda, R., Bertin, X., Guerreiro, M., Fortunato, A.B., Silva, A.M., Andrade, C.,
823 Oliveira, A., Antunes, C., Freitas, M.C., Nahon, A., Rodrigues, M., Bruneau, N., 2011.
824 Medium-term morphodynamic evolution of a small coastal inlet. Journal of Coastal
825 Research, SI 64, 666-670.

826 Gallop, S.L., Bryan, K.R., Coco, G., Stephens, S.A., 2011. Storm-driven changes in rip
827 channel patterns on an embayed beach. Geomorphology, 127 (3-4), 179-188.
828 Gorrel, L., Raubenheimer, B., Elgar, A., Guza, R.T., 2011. SWAN predictions of waves
829 observed in shallow water offshore of complex bathymetry. Coastal Engineering, 58
830 (6), 510-516.
831 Harley, M.D., Turner, I.L., Morris, B.D., Short, A.D., Ranasinghe, R., 2007. Nearshore wave
832 climate and localised erosion during high wave events – SE Asutralia. Proceedings of
833 the 18th Australasian Coastal and Ocean Engineering Conference. IEAust, Melbourne,
834 Australia. No. 89 (CD-ROM).
835 Hasselman, K., Barnett, T.P., Bows, E., Carlson, H., Cartwright, D.E., Enke, K., Ewing, J.A.,
836 Gienapp, H., Hasselman, D.E., Kruseman, P., Meerburg, A., Müller, P., Olbers, D.J.,
837 Richter, K., Sell, W., Walden, H., 1973. Measurements of wind-wave growth and
838 swell decay during the Joint North Sea Wave Project (JONSWAP). Ergänzungsheft
839 zur Deutschen Hydrographischen Zeitschrift, A8 (12), pp. 1-95.
840 Holman, R., Symonds, G., Thornton, E.B., Ranasinghe, R., 2006. Rip spacing and persistence
841 on and embayed beach. Journal of Geophysical Research, 111, C01006.
842 Holthuijsen, L.H., 2007. Waves in Oceanic and Coastal Waters. Cambridge University Press,
843 Cambridge.
844 Huntley, D.A., Hendry, M.D., Jaines, J., Greenidge B., 1988. Waves and rip currents on a
845 Caribbean pocket beach, Jamaica. Journal of Coastal Research, 4 (1), 69-79.
846 Inman, D.L., Elwany, M.H.S., Jenkins, S.A., 1993. Shorerise and Bar-Berm Profiles on Ocean
847 Beaches. Journal of Geophysical Research, 98 (C10), 18181-18199.
848 Lahoz, M.G., Albiach, J.C.C., 2005. Wave forecasting at the Spanish coasts. Journal of
849 Atmospheric & Ocean Science, 10 (4), 389-405.

Lee, G.H., Nicholls, R.J., Birkemeier, W.A., 1998. Storm-driven variability of the beach-nearshore profile at Duck, North Carolina, USA, 1981-1991. Marine Geology, 148 (3-4), 163-177.

Long, J.W., Özkan-Haller, H.T., 2005. Offshore controls on nearshore rip currents. Journal of Geophysical Research, 110 (C12), C12007.

Loureiro, C., Ferreira, Ó., Cooper, J.A.G., 2011. Morphologic change and morphodynamics at high-energy embayed beaches in southwestern Portugal. Proceedings of Coastal Sediments 2011. World Scientific Publishing, Singapore. Vol 2, 1375-1389.

MacMahan, J.H., Thornton, E.B., Stanton, T.P., Reniers, A.J.H.M., 2005. RIPEX: Observations of a rip current system. Marine Geology, 218 (1-4), 113-134.

MacMahan, J.H., Thornton, E.B., Reniers, A.J.H.M., 2006. Rip current review. Coastal Engineering, 53 (2-3), 191-208.

MacMahan, J.H., Thornton, E.B., Reniers, A.J.H.M., Stanton, T.P., Symonds, G., 2008. Low-energy rip currents associated with small bathymetric variations. Marine Geology, 255 (3-4), 156-164.

MacMahan, J.H., Brown, J., Brown, J., Thornton, E., Reniers, A., Stanton, T., Henriquez, M., Gallagher, E., Morrison, J., Austin, M.J., Scott, T.M., Sénéchal, N., 2010. Mean Lagrangian flow behaviout on an open coast rip-channeled beach: a new perspective. Marine Geology, 268 (1-4), 1-15.

McKenzie, P., 1958. Rip-current systems. Journal of Geology, 66 (2), 103-113.

Orzech, M.D., Thornton, E.B., MacMahan, J.H., O'Reilly, W.C., Stanton, T.P., 2010. Alongshore rip channel miigration and sediment transport. Marine Geology, 271 (3-4), 278-291.

Pattiaratchi, C., Olsson, D., Hetzel, Y., Lowe, R., 2009. Wave-driven circulation patterns in the lee of groynes. Continental Shelf Research, 29 (16), 1961-1974.

875 Pita, C., Santos, J.A., 1989. Análise dos temporais da costa oeste de Portugal Continental,
876 Report NATO PO-WAVES 1/89-A. IH/LNEC, Lisboa, Portugal.
877 Ranasinghe, R., Symonds, G., Black, K., Holman, R., 2004. Morphodynamics of intermediate
878 beaches: a video imaging and numerical modelling study. Coastal Engineering, 51 (7),
879 629-655.
880 Short, A.D., 1979. Three dimensional beach-stage model. Journal of Geology, 87 (5), 553-
881 571.
882 Short, A.D., 1985. Rip-current type, spacing and persistence, Narrabeen Beach, Australia.
883 Marine Geology, 65 (1-2), 47-71.
884 Short, A.D. (Ed.), 1999. Handbook of Beach and Shoreface Morphodynamics, John Wiley &
885 Sons, Chichester. 379 pp.
886 Short, A.D., 2007. Australian rip systems: friend or foe?. Journal of Coastal Research, SI 50,
887 7-11.
888 Short, A.D., 2010. Role of geological inheritance in Australian beach morphodynamics.
889 Coastal Engineering, 57 (2), 92-97.
890 Short, A.D., Hesp, P.A., 1982. Wave, beach and dune interaction in Southeastern Australia.
891 Marine Geology, 48 (3-4), 259-284.
892 Short, A.D., Masselink, G. 1999. Embayed and structurally controlled beaches. In: Short,
893 A.D. (Ed.), Handbook of Beach and Shoreface Morphodynamics, John Wiley & Sons,
894 Chichester, pp. 230-249.
895 Silva, R., Baquerizo, A., Losada, M.A., Mendonza, E., 2010. Hydrodynamics of a headland-
896 bay beach – nearshore current circulation. Coastal Engineering, 57 (2), 160-175.
897 Smith, A.M., Mather, A.A., Bundy, S.C., Cooper, J.A.G., Guastella, L.A., Ramsay, P.J.,
898 Theron, A., 2010. Contrasting styles of swell-driven coastal erosion: examples from
899 KwaZulu-Natal, South Africa. Geological Magazine, 147 (6), 940-953.

900 Thom, B.G., 1974. Coastal erosion in Eastern Australia. Search, 5 (5), 198-209.
901 Thom, B.G., Hall, W., 1991. Behaviour of beach profiles during accretion and erosion
902 dominated periods. Earth Surface Processes and Landforms, 16 (2), 113-127.
903 Turner, I.L., Whyte, D., Ruessink, B.G., Ranasinghe, R., 2007. Observations of rip spacing,
904 persistence and mobility at a long, straight coastline. Marine Geology, 236 (3-4), 209-
905 221.
906 Wood, D.J., Muttray, M., Oumeraci, H., 2001. The SWAN model used to study wave
907 evolution in a flume. Ocean Engineering, 28 (7), 805-823.
908 Wright, L.D., 1981. Beach cut in relation to surf zone morphodynamics. Proceedings of the
909 17th International Conference on Coastal Engineering. ASCE, Sydney, Australia, pp.
910 978-996.
911 Wright, L.D., Short, A.D., 1983. Morphodynamics of beaches and surf zones in Australia. In:
912 Komar, P.D. (Ed.), CRC Handbook of Coastal Processes and Erosion. CRC Press,
913 Boca Raton, Florida, pp. 35-64.
914 Wright, L.D., Short, A.D., 1984. Morphodynamic variability of surf zones and beaches - a
915 synthesis. Marine Geology, 56 (1-4), 93-118.
916 Wright, L.D., Thom, B.G., Chappell, J., 1979. Morphodynamic variability of high-energy
917 beaches. Proceedings of the 16th International Conference on Coastal Engineering.
918 ASCE, Hamburg, Germany, pp. 1180-1194.
919
920
921
922
923
924

LIST OF TABLES

Table 1

Mean offshore wave conditions used in model runs and corresponding alongshore averaged breaking wave heights ($H_{b\bar{y}}$) and standard deviation ($H_{b\sigma}$) for Arrifana, Mt. Clérigo and Amoreira embayments. Grey shading highlights modal conditions.

Table 2

Characteristics of observed storms from different directions used for model runs. Values of H_{so}, T_p and θ are time averages for the duration of each event.

Table 3

Geometric and morphodynamic characteristics of the embayments.

LIST OF FIGURES

Fig. 7. Time series of offshore significant wave height (H_{so}) (top panel) and cumulative volume changes for Mt. Clérigo beach profiles (black solid line in lower panels). Refer to Fig. 6 caption for description of symbols. **B&W web and printing**

Fig. 8. Time series of offshore significant wave height (H_{so}) (top panel) and cumulative volume changes for Amoreira beach profiles (black solid line in lower panels). Refer to Fig. 6 caption for description of symbols. **B&W web and printing**

Fig. 9. Alongshore variation in breaking wave height (H_b) for each embayment. Wave conditions were modelled for the storms identified in Table 2 (left panel) and for synthetic storms (right panel). Synthetic storms have constant offshore wave height (5 m) and peak period (15 s), but variable offshore wave directions of 315º (NW), 270º (W) and 225º (SW). Profile location is represented by grey vertical lines. **B&W web and printing**

Fig. 10. Modelled significant wave height (H_s) for the average conditions recorded during the January-February 2009 storm group (offshore boundary conditions: H_{so} - 4.5 m; T_p - 14.5 s; θ - 300º), at Arrifana (top panel), Mt. Clérigo (centre panel) and Amoreira (bottom panel). Depth contours (dotted lines) are in metres below MSL, and black lines indicate profile location. **Colour web and printing**

Fig. 11. Embayment scaling parameter (δ') for different alongshore averaged breaking wave heights ($H_{b\bar{y}}$) in each embayment (refer to Table 1). Shading highlights modal conditions at each embayment. **B&W web and printing**

Fig. 12. Panoramic mosaics of megarip circulation during storm and post-storm wave conditions for Arrifana. The upper panel presents the embayment under storm conditions, recorded on 05/02/2009 under 5.5 m WNW offshore waves. Arrows provide flow-behaviour indications of the megarips, and dashed lines indicate rip head plumes. The intense wave breaking across the entire surfzone is reduced within the rip-neck channel due to wave-current interaction. Post-storm conditions, recorded on 09/02/2009, are shown in the lower panel. Dark patches and the absence of wave breaking on both beach extremities indicate the position of the feeder channels and deep rip-neck channels. **Colour web and printing**

Fig. 13. Schematic mapping of megarip circulations during storm (left panel) and post-storm conditions (right panel) for Arrifana embayment. Rip neck channels (limited by solid black lines) are indicated for both storm and post storm conditions; while feeder channels (limited by dashed black line) are only clearly identifiable during post-storm conditions (refer to Figure 12 for snapshot view). Arrows indicate flow direction only and are not scaled to velocity, and bathymetry is in metres below MSL. **B&W web and printing**

Fig. 14. Schematic mapping of megarip circulations during storm (left panel) and post-storm conditions (right panel) for Mt. Clérigo embayment. Refer to Fig. 13 caption for description of symbols. **B&W web and printing**

Fig. 15. Schematic mapping of megarip circulations during storm (left panel) and post-storm conditions (right panel) for Amoreira embayment. Refer to Fig. 13 caption for description of symbols. **B&W web and printing**

Table 1
Mean offshore wave conditions used in model runs and corresponding alongshore averaged breaking wave heights ($H_{b\bar{y}}$) and standard deviation ($H_{b\sigma}$) for Arrifana, Mt. Clérigo and Amoreira embayments. Grey shading highlights modal conditions.

H_{so} Classes	Mean offshore conditions			Arrifana		Mt. Clérigo		Amoreira	
	H_{so} (m)	T_p (s)	θ (º)	$H_{b\bar{y}}$ (m)	$H_{b\sigma}$ (m)	$H_{b\bar{y}}$ (m)	$H_{b\ \sigma}$ (m)	$H_{b\bar{y}}$ (m)	$H_{b\ \sigma}$ (m)
0.5 – 1.0	0.81	9.4	297	0.55	0.08	0.87	0.04	0.82	0.09
1.0 – 1.5	1.26	10.1	300	0.88	0.12	1.43	0.04	1.37	0.09
1.5 – 2.0	1.73	11.2	302	1.03	0.14	1.66	0.05	1.62	0.08
2.0 – 2.5	2.22	12.0	301	1.47	0.20	2.38	0.04	2.33	0.08
2.5 – 3.0	2.75	12.6	299	1.94	0.27	3.08	0.02	3.05	0.03
3.0 – 3.5	3.21	12.9	299	2.20	0.31	3.48	0.02	3.45	0.03
3.5 – 4.0	3.76	13.5	297	2.38	0.35	3.74	0.03	3.71	0.03
4.0 – 4.5	4.26	14.2	297	2.57	0.36	4.00	0.03	3.97	0.03
4.5 – 5.0	4.73	14.2	294	2.82	0.42	4.35	0.03	4.32	0.03
5.0 – 5.5	5.23	14.6	294	3.18	0.48	4.88	0.03	4.86	0.03
5.5 – 6.0	5.75	15.2	296	3.74	0.59	5.75	0.04	5.73	0.04
6.0 – 6.5	6.25	15.3	298	4.03	0.67	6.25	0.04	6.23	0.05
6.5 – 7.0	6.63	15.7	297	4.39	0.77	6.80	0.05	6.79	0.05
> 7.0	7.82	17.1	298	4.62	0.85	7.23	0.05	7.22	0.06

Table 2
Characteristics of observed storms from different directions used for model runs. Values of H_{so}, T_p and θ are time averages for the duration of each event.

Storm	**WNW**	**W**	**WSW**
Start date	14/12/2008	01/02/2009	10/04/2008
Duration (hours)	15	32	5
H_{so} (m)	5.16	5.50	5.31
T_p (s)	13.8	13.6	11.9
θ (º from North)	309	275	241

Table 3

Geometric and morphodynamic characteristics of the embayments.

Parameters	**Arrifana**	**Mt. Clérigo**	**Amoreira**
Embayment shoreline length (m)	2050	950	820
Embayment width (m)	1340	780	570
Beachface slope (º)	2.2	2.0	1.3
Modal H_b (m)	1.03	1.66	1.62
Modal δ'	30	7	7

Figure 1

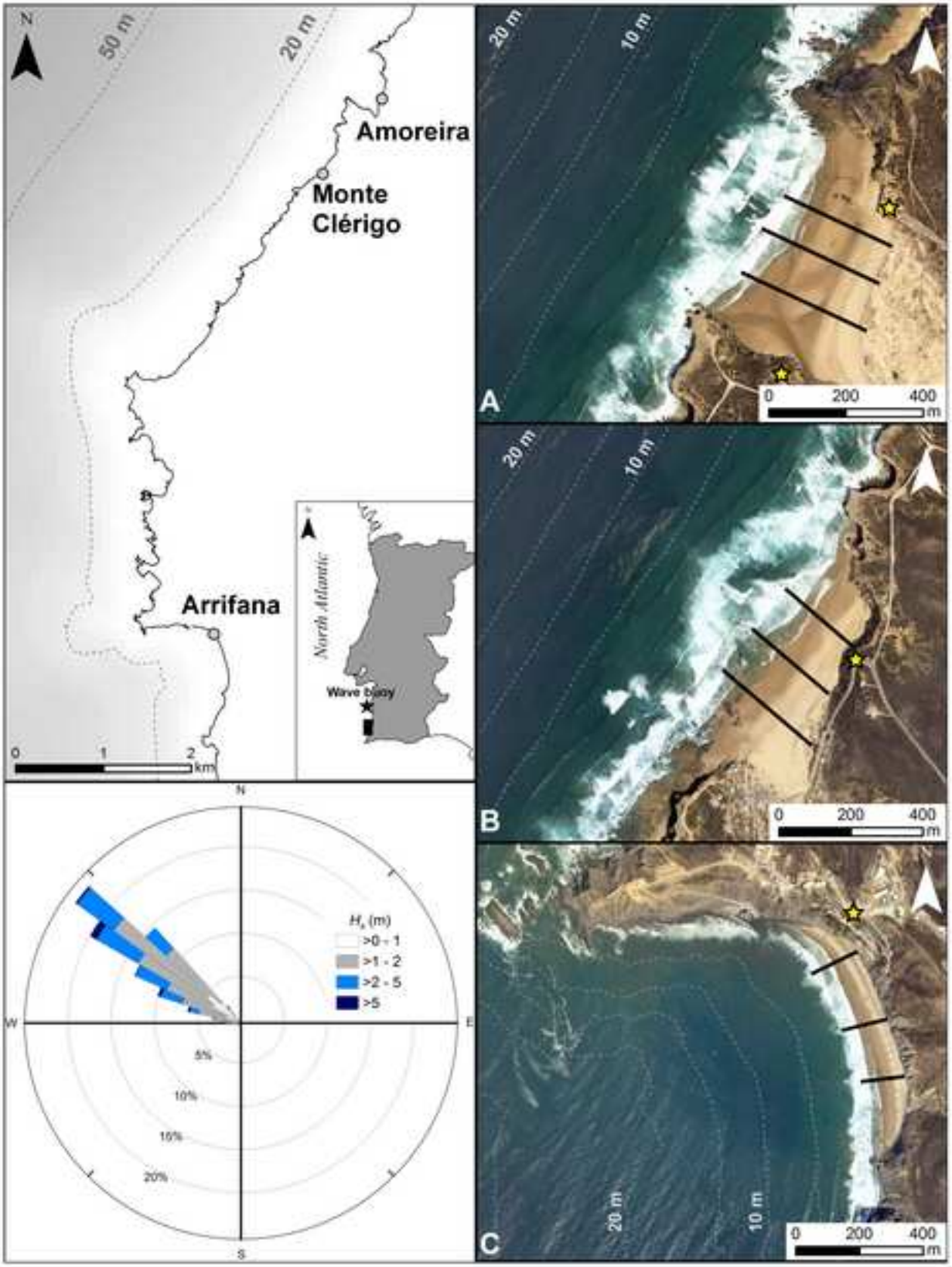
N
50 m
20 m
Amoreira
Monte
Clérigo
Arrifana
0
1
2
km
North Atlantic
Wave buoy
N
W
E
S
5%
10%
15%
20%
H_s (m)
>0 - 1
>1 - 2
>2 - 5
>5
20 m
10 m
A
0
200
400
m
B
C

Figure 2

Profile and rip interaction / Parameters	Profile intersected or immediately adjacent to rip-neck channel	Profile intersected or immediately adjacent to feeder channel	Profile without influence of rip-neck or feeder channels
Morphologic relief - descrition	- sharply inflected slope - abrupt deepening - cross-shore incision	- intertidal trough - bar seaward of trough - alongshore incision	- linear to concave slope - smooth deepening - no channel incision
Morphologic relief - cross-shore intertidal profile with (below) and without (above) terrace	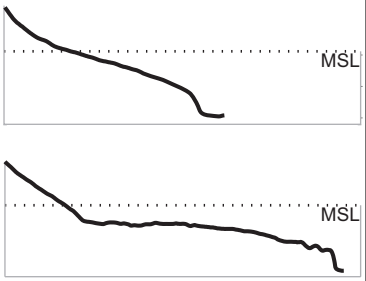	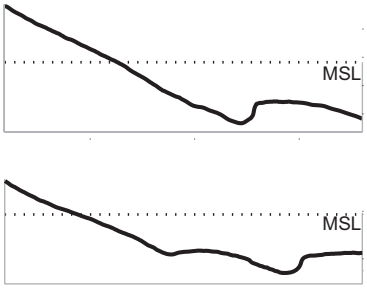	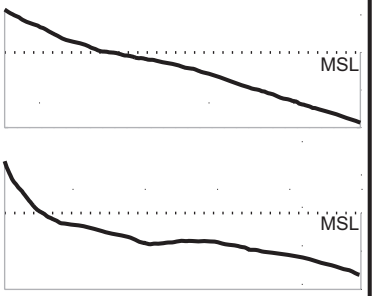
Visual signature - description	- cross-shore orientation - gaps in breaking line - foam seaward of breakers	- alongshore orientation - streaks of darker water - breaking in the bar seaward of trough	- along and cross-shore uniformity - homogenous bores - regular breaking line
Visual signature - photography			
Boundary diagram	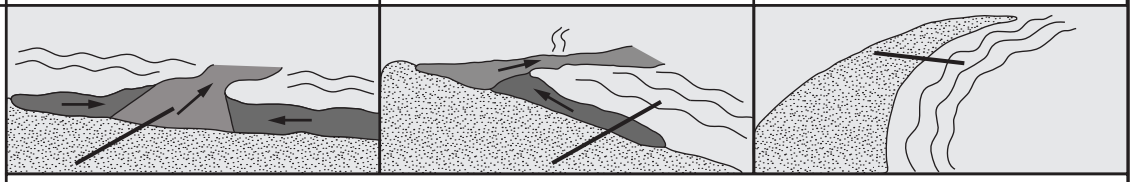		
Flow direction	- offshore directed	- alongshore directed	- onshore directed

Figure 3

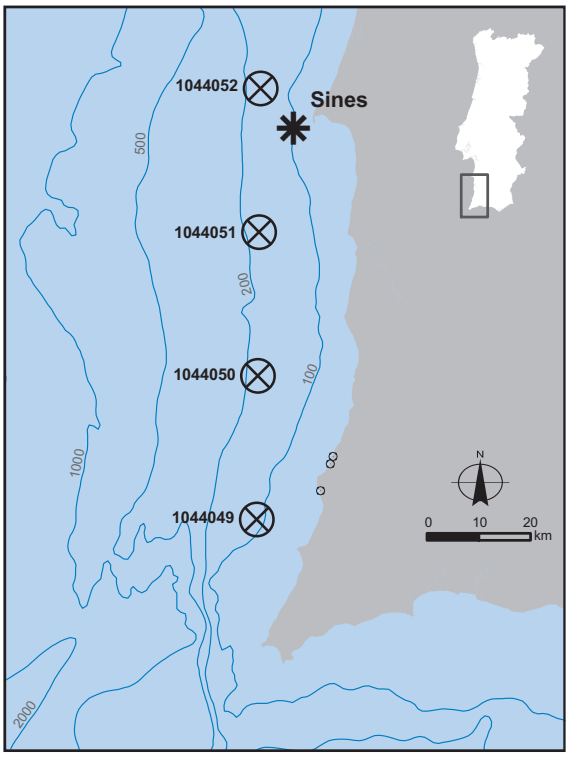
1044052
Sines
500
1044051
200
1044050
100
1000
0
00
1044049
N
0
10
20
km
2000

Figure 4

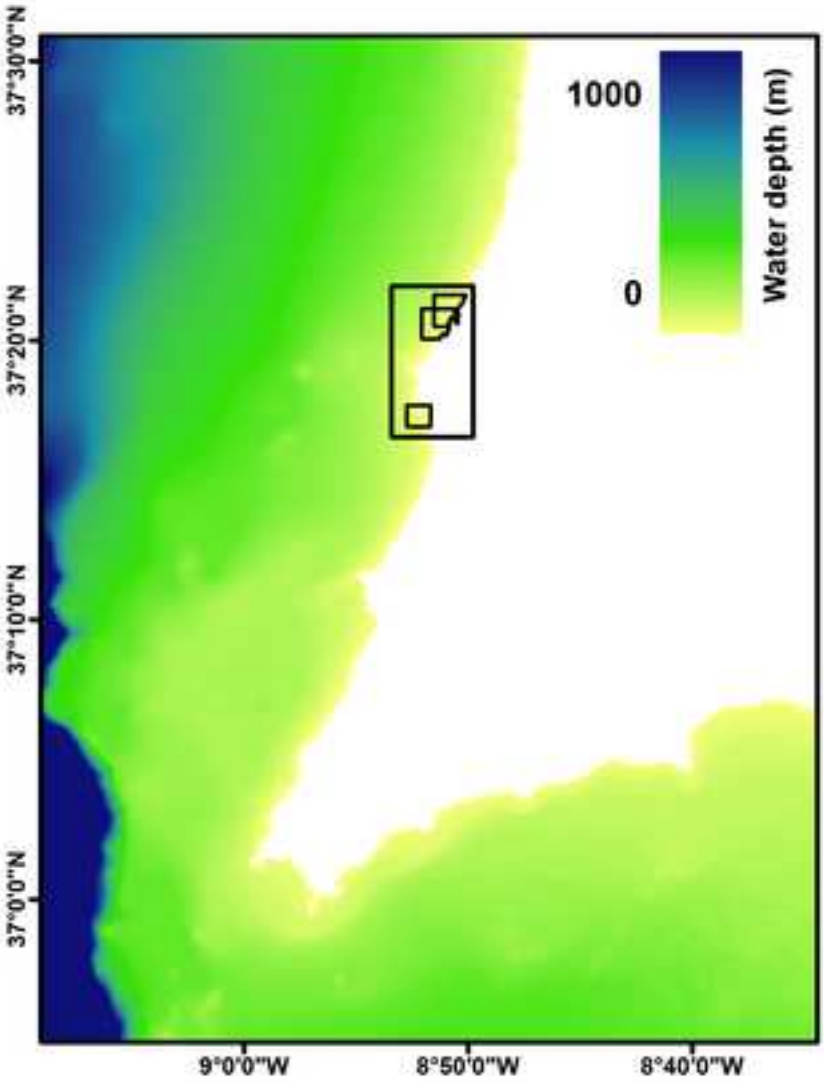
37°30'0"N
37°20'0"N
37°10'0"N
37°0'0"N
9°0'0"W
8°50'0"W
8°40'0"W
1000
0
Water depth (m)

Figure 5

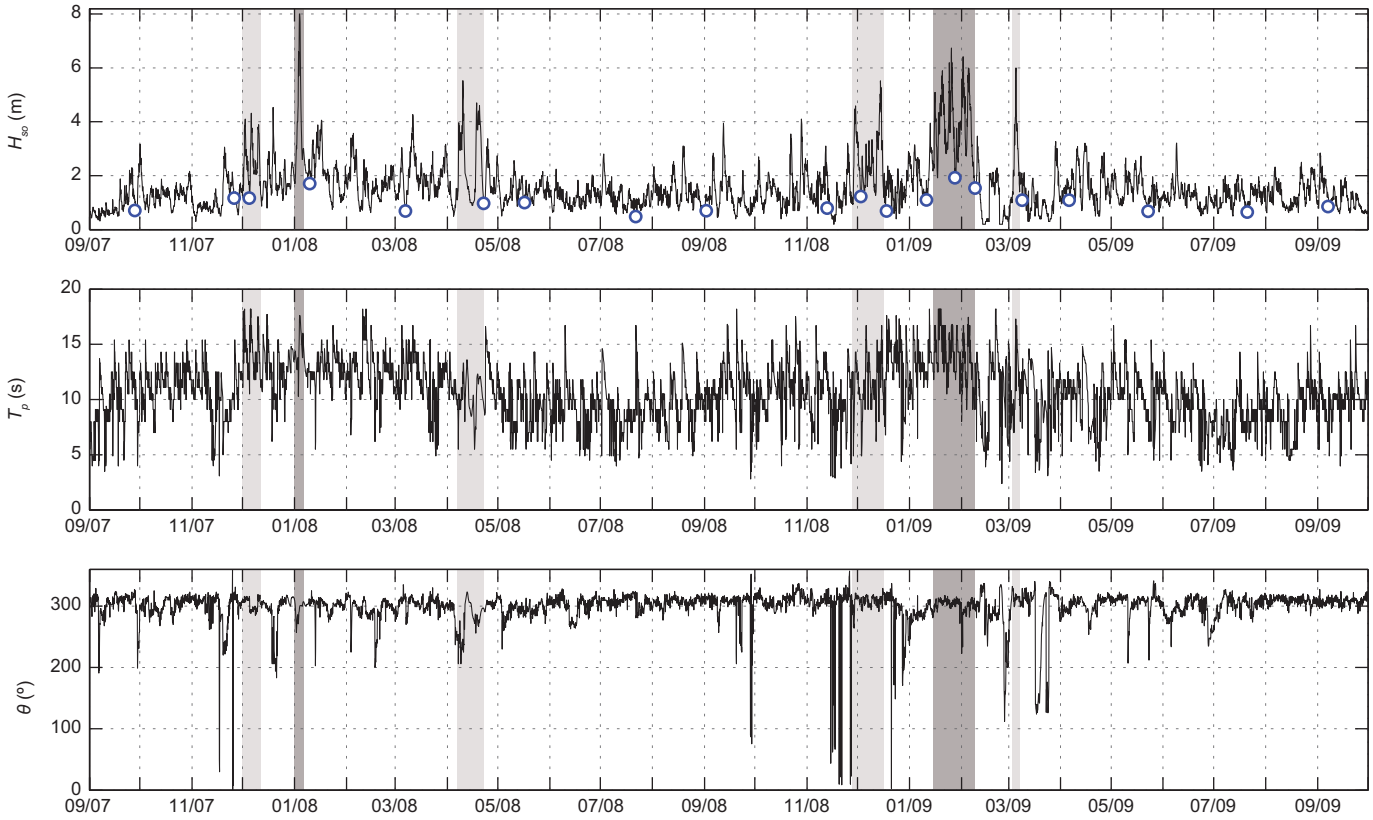
H_{so} (m)
8
6
4
2
0
T_p (s)
20
15
10
5
0
θ (°)
300
200
100
0
09/07
11/07
01/08
03/08
05/08
07/08
09/08
11/08
01/09
03/09
05/09
07/09
09/09

Figure 6

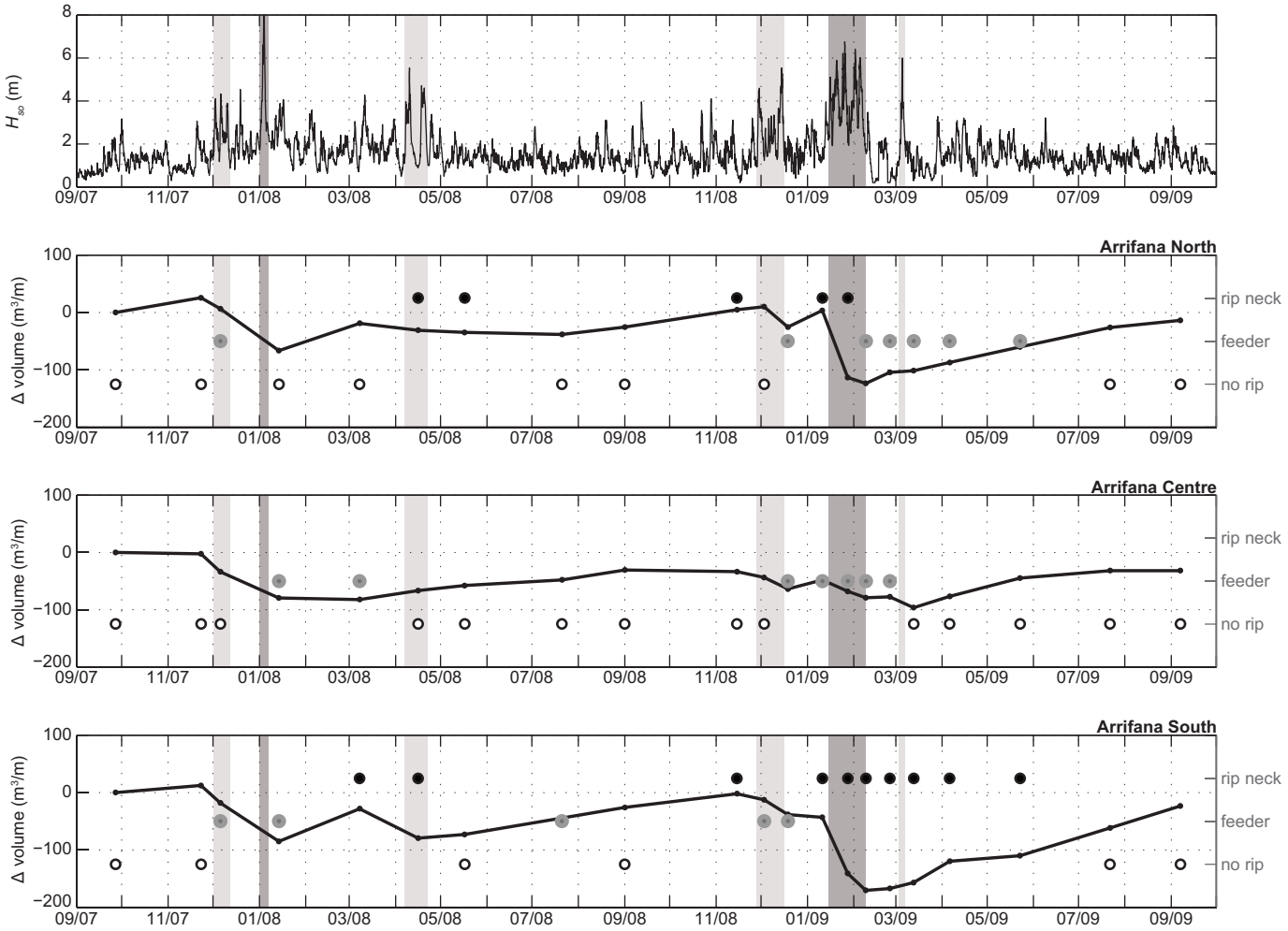
H_{s0} (m)
8
6
4
2
0
09/07
11/07
01/08
03/08
05/08
07/08
09/08
11/08
01/09
03/09
05/09
07/09
09/09
Arrifana North
Arrifana Centre
Arrifana South
Δ volume (m³/m)
100
0
−100
−200
rip neck
feeder
no rip

Figure 7

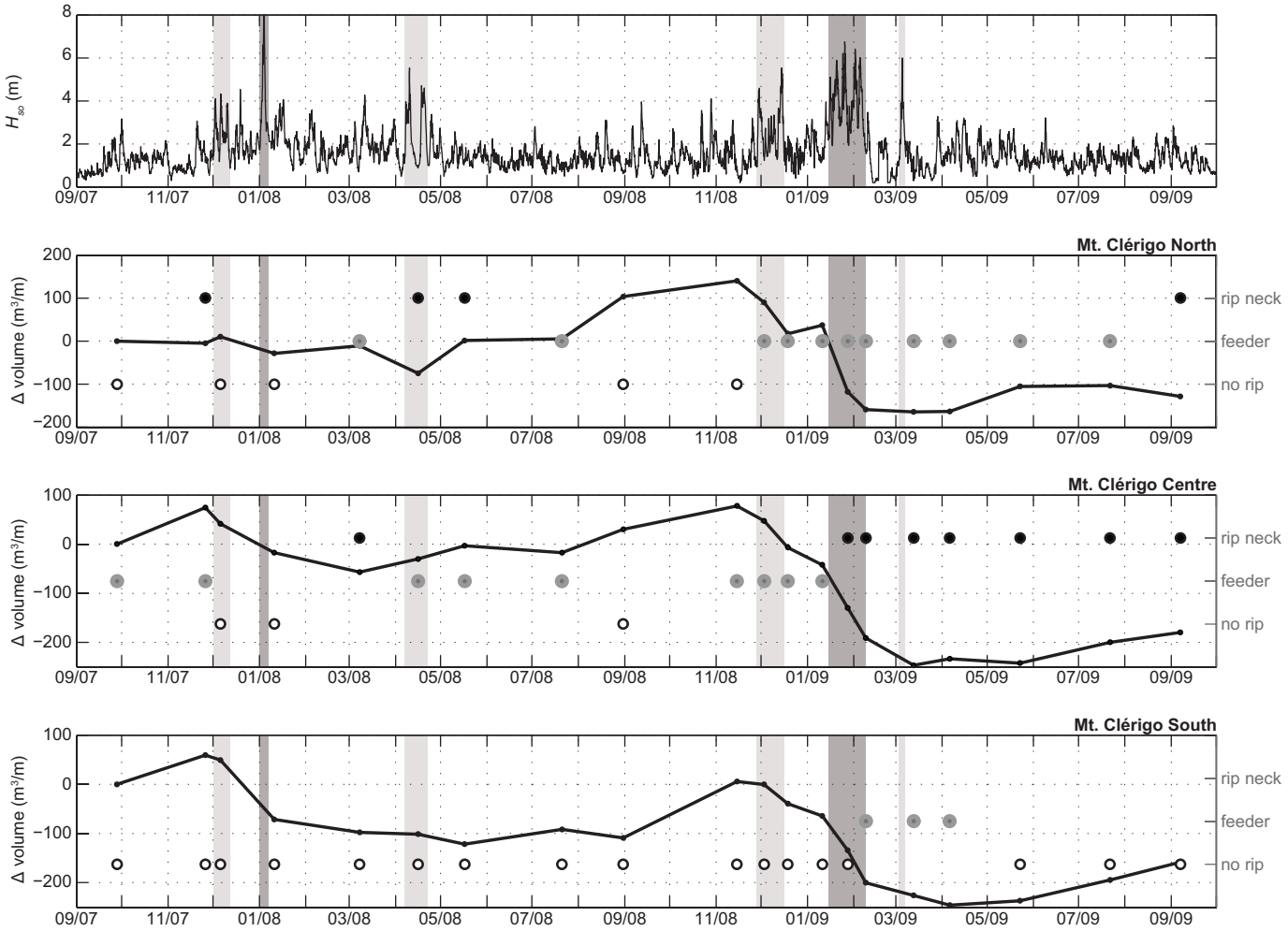
H_{so} (m)
Δ volume (m³/m)
Mt. Clérigo North
Mt. Clérigo Centre
Mt. Clérigo South
rip neck
feeder
no rip
09/07
11/07
01/08
03/08
05/08
07/08
09/08
11/08
01/09
03/09
05/09
07/09
09/09

Figure 8

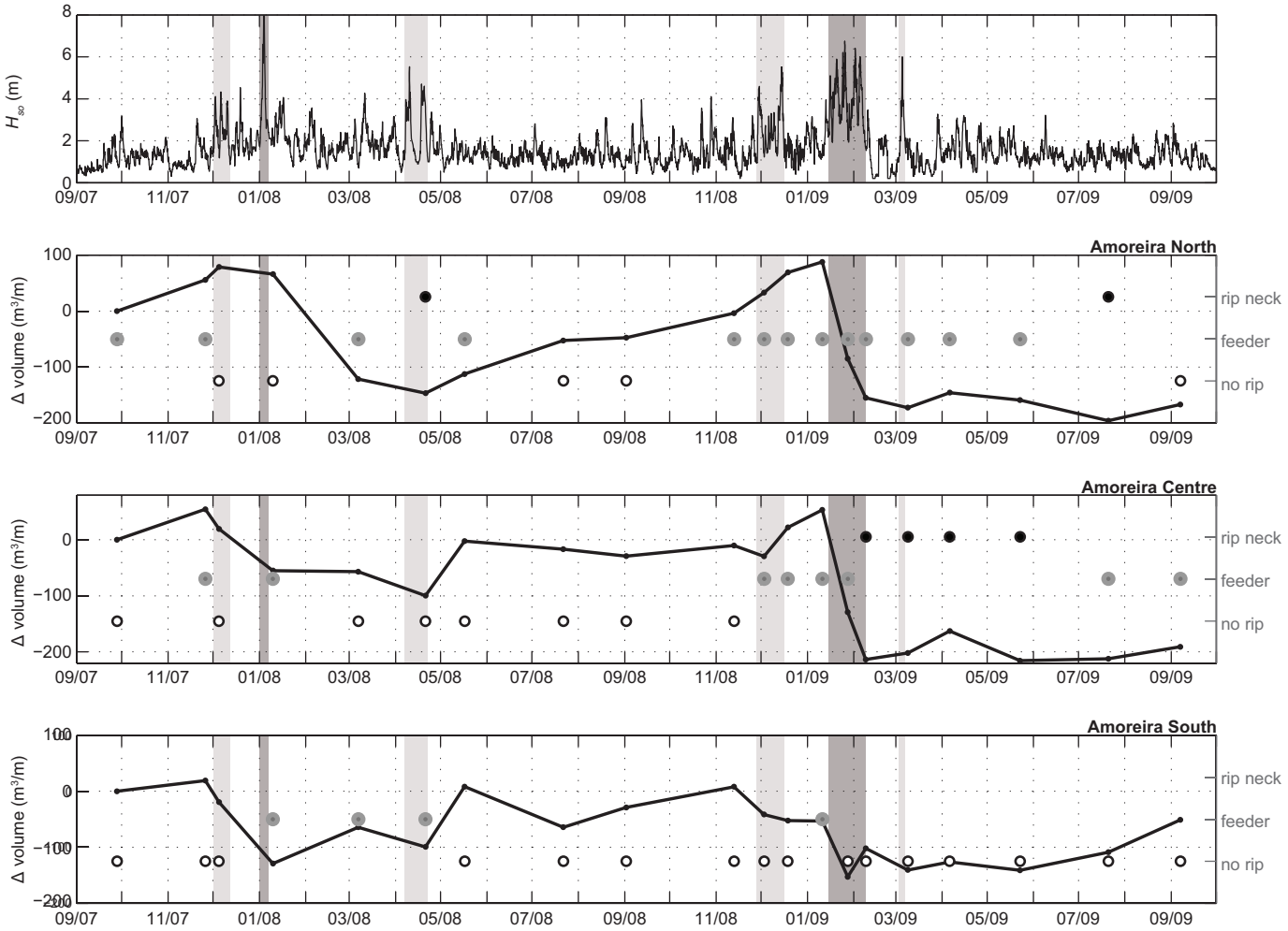
H_{s0} (m)
8
6
4
2
0
09/07
11/07
01/08
03/08
05/08
07/08
09/08
11/08
01/09
03/09
05/09
07/09
09/09
Amoreira North
Amoreira Centre
Amoreira South
Δ volume (m³/m)
100
0
−100
−200
rip neck
feeder
no rip

Figure 9

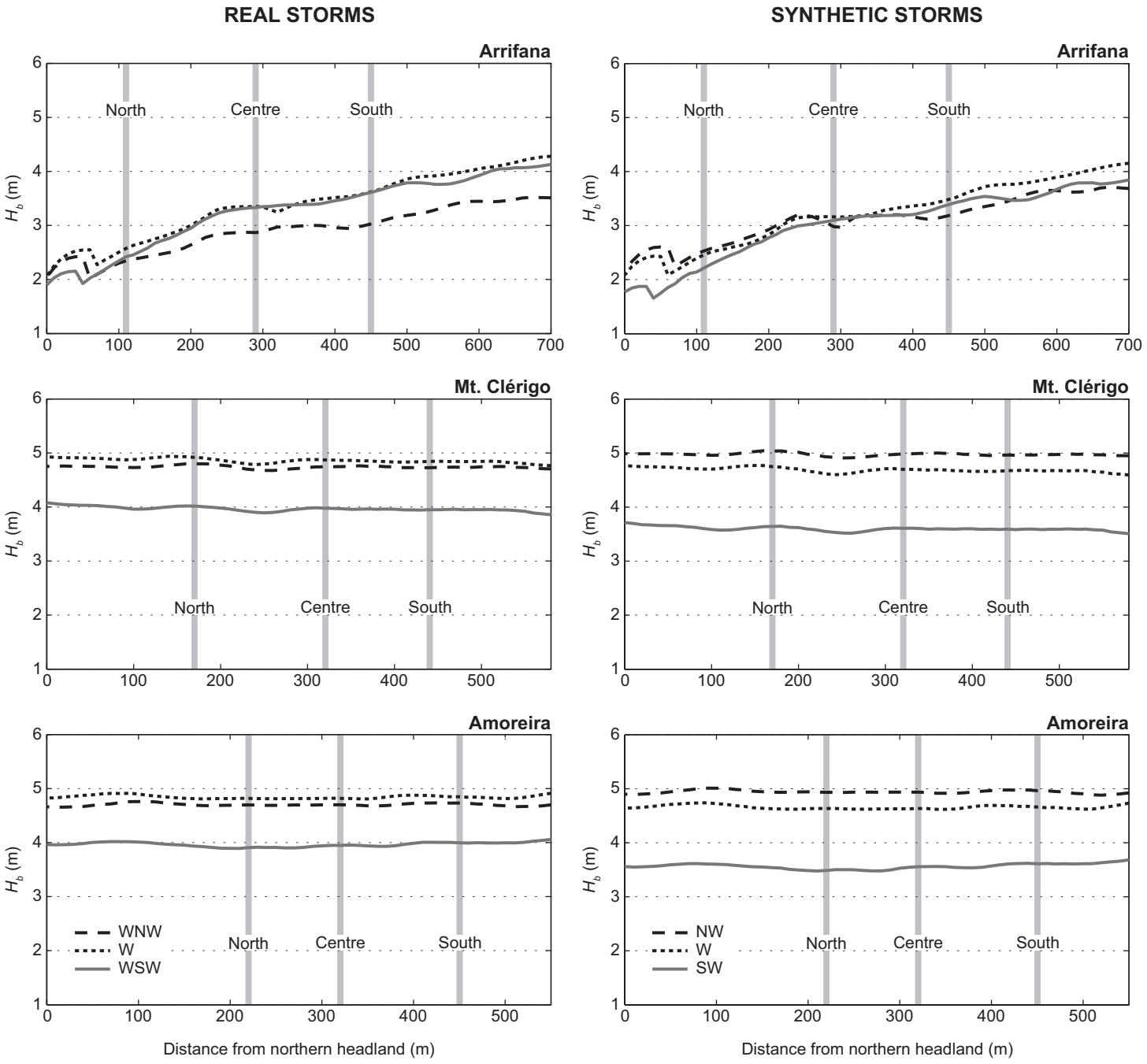
REAL STORMS
SYNTHETIC STORMS
Arrifana
Mt. Clérigo
Amoreira
North
Centre
South
H_b (m)
WNW
W
WSW
NW
SW
Distance from northern headland (m)

Figure 10

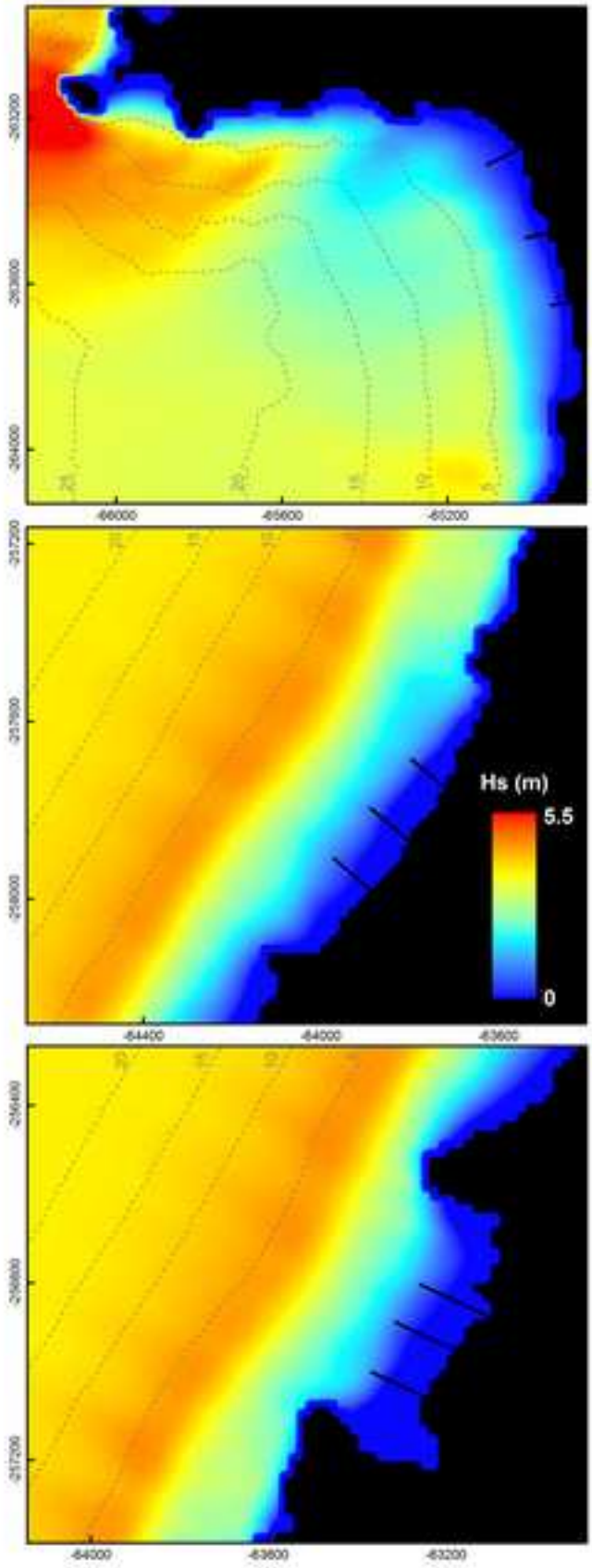

Figure 11

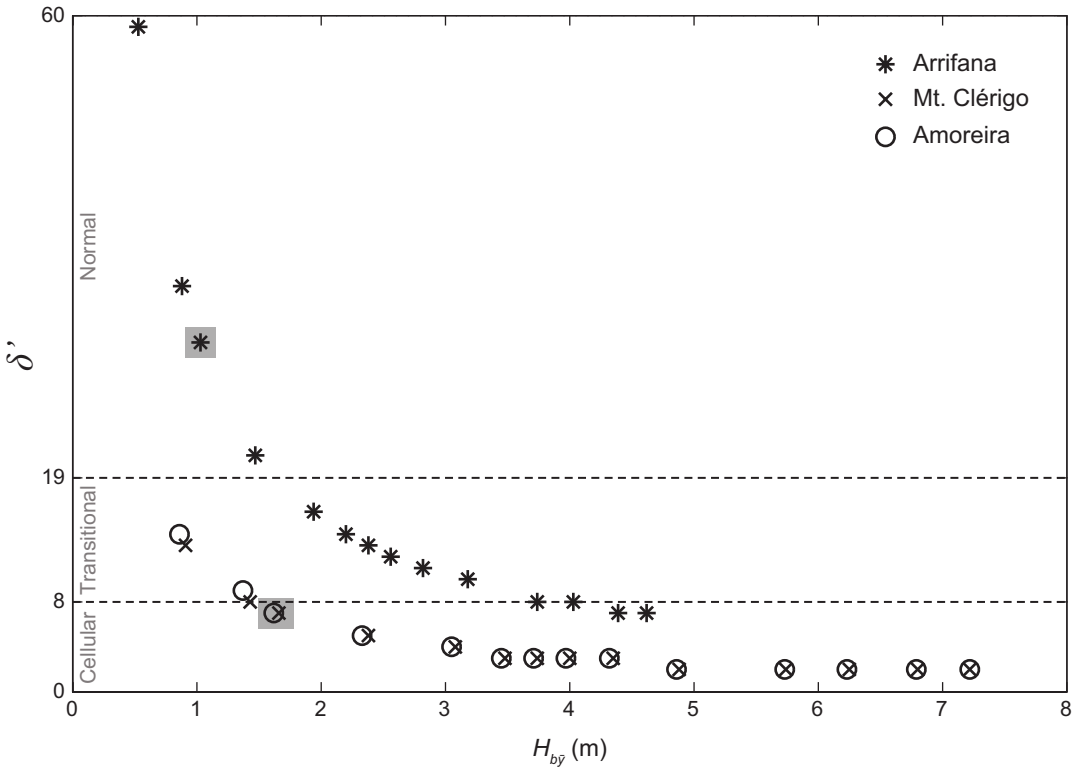
60
19
8
0
0
1
2
3
4
5
6
7
8
δ'
$H_{b\bar{y}}$ (m)
Normal
Transitional
Cellular
Arrifana
Mt. Clérigo
Amoreira

Figure 12

Figure 13

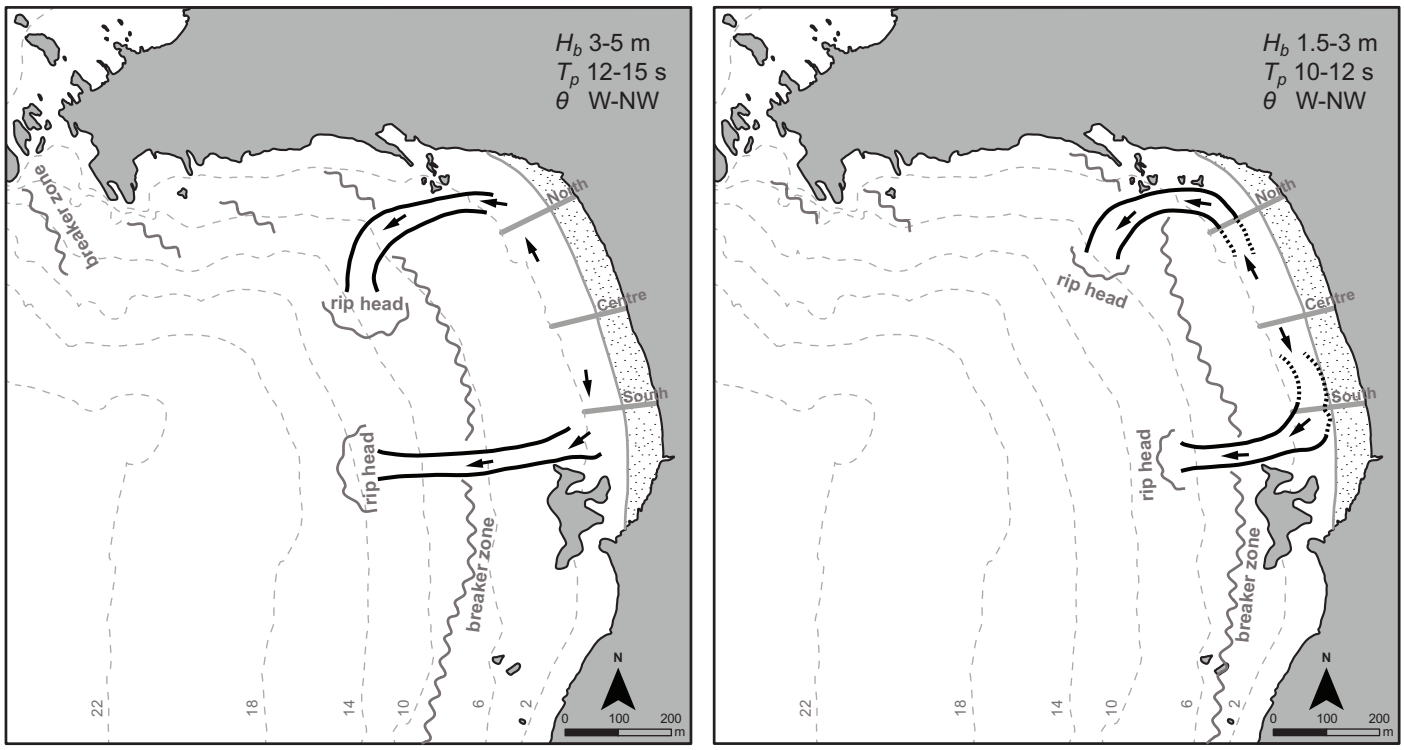
H_b 3-5 m
T_p 12-15 s
θ W-NW
breaker zone
rip head
North
Centre
South
rip head
breaker zone
22
18
14
10
6
2
N
0
100
200
m
H_b 1.5-3 m
T_p 10-12 s
θ W-NW
rip head
North
Centre
South
rip head
breaker zone
22
18
14
10
6
2
N
0
100
200
m

Figure 14

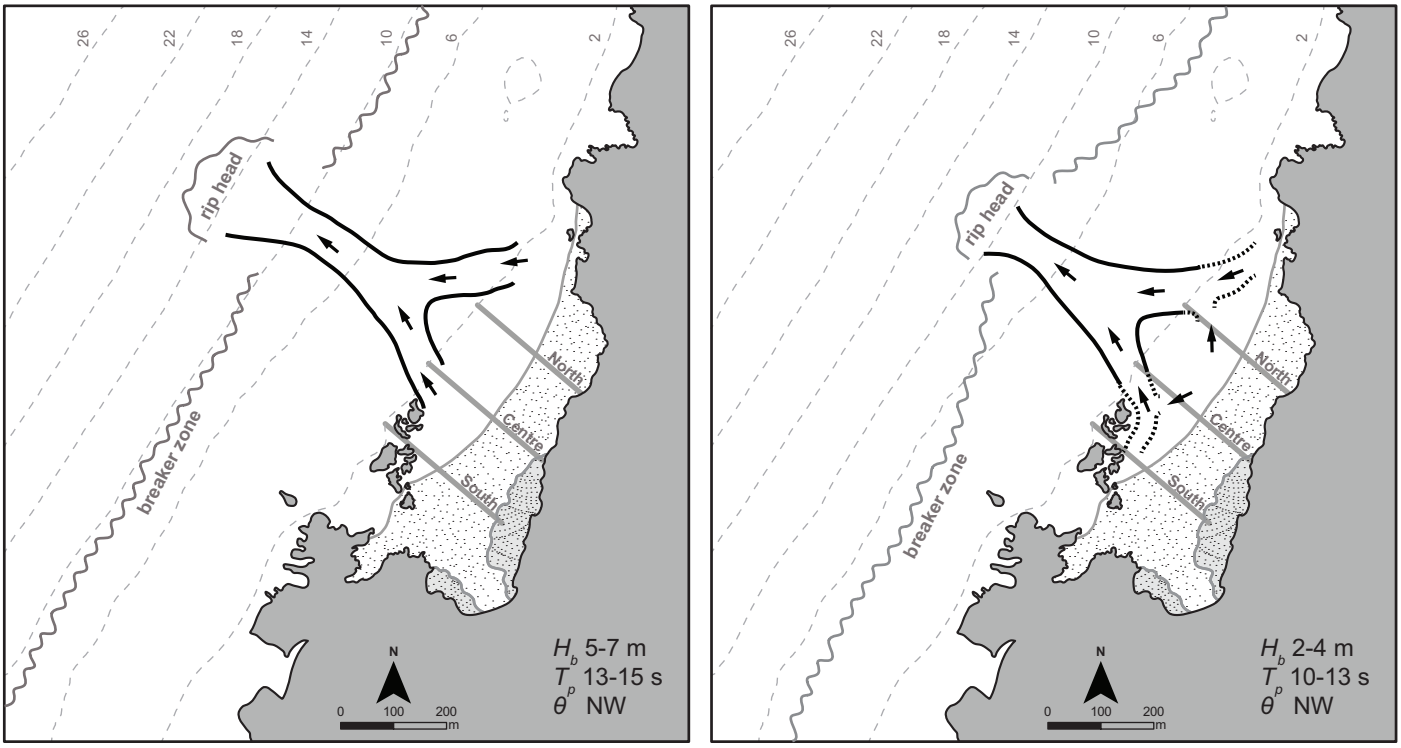
26
22
18
14
10
6
2
rip head
breaker zone
North
Centre
South
N
0
100
200
m
H_b 5-7 m
T_p 13-15 s
θ^p NW
H_b 2-4 m
T_p 10-13 s
θ^p NW

Figure 15

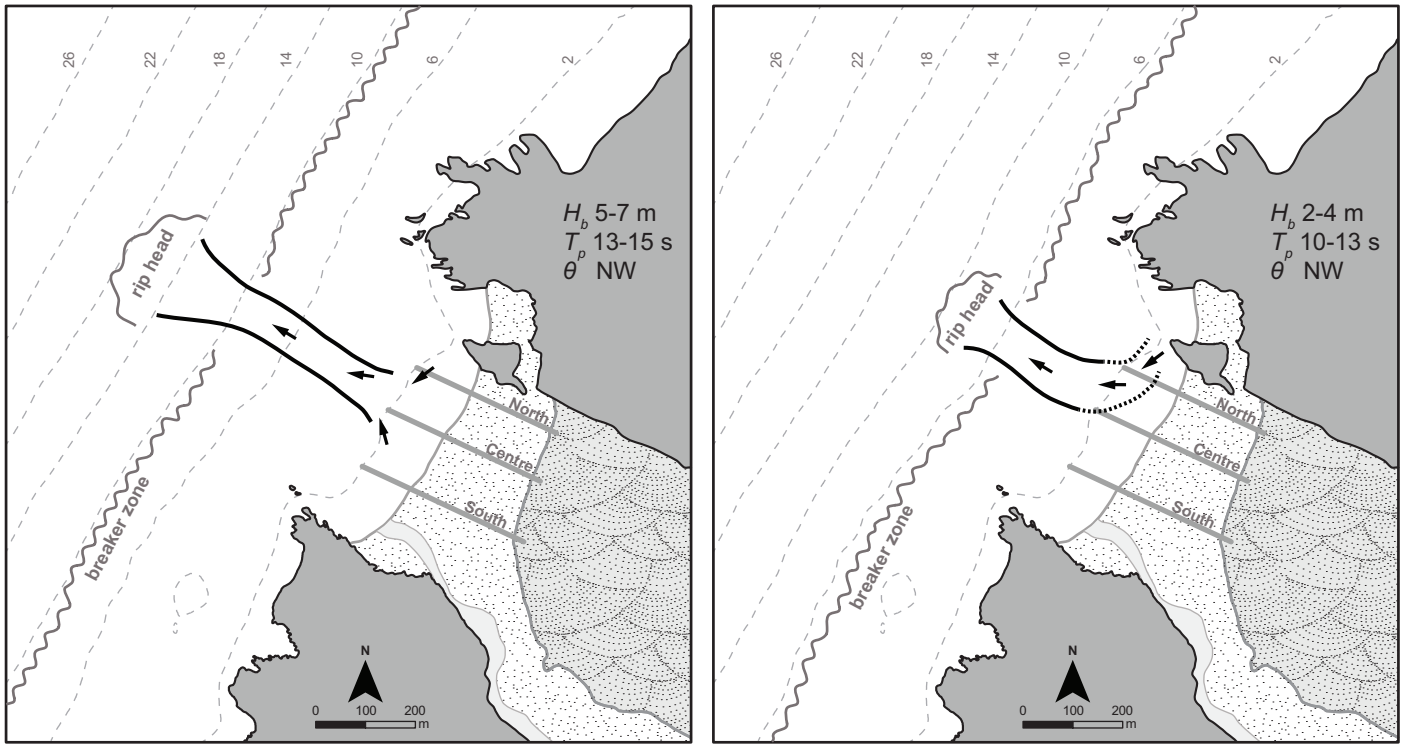
26
22
18
14
10
6
2
rip head
breaker zone
H_b 5-7 m
T_p 13-15 s
θ NW
North
Centre
South
N
0 100 200
m
26
22
18
14
10
6
2
rip head
breaker zone
H_b 2-4 m
T_p 10-13 s
θ NW
North
Centre
South
N
0 100 200
m